OULU 2019
C 712

ACTA UNIVERSITATIS OULUENSIS

Eshwar Kumar Ramasetti

MODELLING OF OPEN-EYE FORMATION AND MIXING PHENOMENA IN A GAS-STIRRED LADLE FOR DIFFERENT OPERATING PARAMETERS

UNIVERSITY OF OULU GRADUATE SCHOOL;
UNIVERSITY OF OULU,
FACULTY OF TECHNOLOGY

ACTA UNIVERSITATIS OULUENSIS
C Technica 712

ESHWAR KUMAR RAMASETTI

MODELLING OF OPEN-EYE FORMATION AND MIXING PHENOMENA IN A GAS-STIRRED LADLE FOR DIFFERENT OPERATING PARAMETERS

Academic dissertation to be presented, with the assent of the Doctoral Training Committee of Technology and Natural Sciences of the University of Oulu, for public defence in the Arina auditorium (TA105), Linnanmaa, on 25 October 2019, at 12 noon

UNIVERSITY OF OULU, OULU 2019

Acta Univ. Oul. C 712, 2019

Supervised by
Professor Timo Fabritius
Doctor Petri Sulasalmi
Doctor Ville-Valtteri Visuri

Reviewed by
Professor Yaowei Yu
Associate Professor Karl Mickael Erik Ersson

Opponent
Docent Mikko Ilmari Helle

ISBN 978-952-62-2355-1 (Paperback)
ISBN 978-952-62-2356-8 (PDF)

ISSN 0355-3213 (Printed)
ISSN 1796-2226 (Online)

Cover Design
Raimo Ahonen

JUVENES PRINT
TAMPERE 2019

Ramasetti, Eshwar Kumar, Modelling of open-eye formation and mixing phenomena in a gas-stirred ladle for different operating parameters.

University of Oulu Graduate School; University of Oulu, Faculty of Technology
Acta Univ. Oul. C 712, 2019
University of Oulu, P.O. Box 8000, FI-90014 University of Oulu, Finland

Abstract

In ladle metallurgy, gas stirring and the behaviour of the slag layer are very important for alloying and the homogenization of the steel. When gas is injected through a nozzle located at the bottom of the ladle into the metal bath, the gas jet exiting the nozzle breaks up into gas bubbles. The rising bubbles break the slag layer and create an open-eye. The size of the open-eye is very important as the efficiency of the metal-slag reactions depend on the interaction between the slag and steel created during the stirring process, and information about the position and size of the open-eye is important for effective alloying practice. Moreover, the open-eye has an effect on the energy balance since it increases heat losses.

In this study, experimental measurements and numerical simulations were performed to study the effect of different operating parameters on the formation of the open-eye and mixing time in a water model and industrial ladle. Experimental measurements were performed to study the effect of the gas flow rate, slag layer thickness, slag layer densities and number of porous plugs in a 1/5 scale water model and in a 150-ton steelmaking ladle. For numerical modelling, a multi-phase volume of fluid (VOF) model was used to simulate the system including the behaviour of the slag layer. The numerical simulation of the open-eye size and mixing time was found to be in good agreement with the experimental data obtained from the water model and data obtained from the industrial measurements.

Keywords: computational fluid dynamics (CFD), ladle stirring, open-eye, slag layer, volume of fluid (VOF) model

Ramasetti, Eshwar Kumar, Avoimen silmäkkeen muodostumisen mallintaminen kaasuhuuhdellussa senkassa.
Oulun yliopiston tutkijakoulu; Oulun yliopisto, Teknillinen tiedekunta
Acta Univ. Oul. C 712, 2019
Oulun yliopisto, PL 8000, 90014 Oulun yliopisto

Tiivistelmä

Senkkametallurgiassa kaasuhuuhtelu ja kuonakerroksen käyttäytyminen ovat tärkeitä teräksen seostamisen ja homogenisoinnin näkökulmasta. Senkan pohjalla sijaitsevasta suuttimesta puhallettava kaasu hajoaa kupliksi, jotka rikkovat kuonakerroksen ja muodostavat avoimen silmäkkeen. Avoimen silmäkkeen koko on yhteydessä voimakkaampaan kuonan emulgoitumiseen, joka tehostaa metallisulan ja kuonan välisiä reaktioita. Tietoa avoimen silmäkkeen paikasta ja koosta tarvitaan myös tehokkaaseen seostuspraktiikkaan. Avoin silmäke vaikuttaa lisäksi prosessin energiataseeseen lisäten sen lämpöhäviöitä.

Tässä tutkimuksessa tutkittiin kokeellisesti ja laskennallisesti erilaisten operointiparametrien vaikutusta avoimen silmäkkeen muodostumiseen vesimallissa ja terässenkassateollisessa senkassa. Kokeellisia mittauksia tehtiin kaasuhuuhtelun, kuonakerroksen paksuuden, ja suuttimien määrän vaikutuksen tutkimiseksi 1/5-mittakaavan vesimallissa ja 150 tonnin terässenkassa. Numeerisessa mallinnuksessa systeemin ja siihen lukeutuvan kuonakerroksen käyttäytymisen simuloimiseen käytettiin volume of fluid (VOF) -monifaasimenetelmää. Avoimen silmäkkeen kokoon ja sekoittumisaikaan liittyvien numeeristen simulointien havaittiin vastaavan hyvin vesimallista ja teollisista mittauksista saatua kokeellista aineistoa.

Asiasanat: avoin silmäke, kuonakerros, laskennallinen virtausdynamiikka (CFD), sekundäärimetallurgia, volume of fluid (VOF) -malli

Dedicated to my father Ramisetti Nageshwara Rao (Late)

Acknowledgements

The research for this thesis was conducted in 2016-2019 at the Process Metallurgy Research Unit at the University of Oulu. The work was funded by the European Commission under grant number 675715-MIMESIS-H2020-MSCA-ITN-2015, which is part of the Marie Sklodowska-Curie Actions Innovative Training Networks European Industrial Doctorate Programme.

I would like to thank my supervisors Professor Timo Fabritius, Dr. Petri Sulasalmi and Dr. Ville-Valtteri Visuri for their guidance and encouragement. I would like to thank Mr. Riku Mattila for his support in all matters during the doctoral studies. I would also like to extend my special thanks to Mr. Jari Savolainen and Mr. Esa Puukko for their support and supervision during the seventeen-month industrial training at Outokumpu Stainless Oy. I would also like thank Professor Dietmar Hömberg and Dr. Thomas Petzold for their support during the three-month secondment period at the WIAS institute in Germany. I would like also to thank Associate Professor Shao Lei and Dr. Mingming Lei for their support during the three-month period at the Northeastern University in China. I would also like to acknowledge Seppo Ollila for his support during the one-month training at SSAB Europe Oy. I would also like to acknowledge Sapotech Oy for their support in capturing the process using IR camera.

Pre-examiners Associate Professor Mikael Ersson and Professor Yaowei Yu are acknowledged for their valuable comments concerning this thesis.

Finally, I would like to thank my parents, my mother Padma, my late father Nageshwara Rao, my sister Nanitha and my dear wife Nikitha Shruthi for their encouragement throughout these years and for supporting me to complete doctoral studies. I would also like to thank my friends Satish Kolli, Vahid Javaheri, Prem Seelam, Vijay Nayani, Suresh Kodukula, Ganapathy Raman, Srikanth Kyatham, Mani Bhowmik, Bala Kumar, Avishek Gupta, Atul Mahajan, Vamsikrishna Akinapalli, Praneeth Susarla, Tun Tun Nyo, Siva Ariram, Abhinay Pandya, Tirthankar Paul, Snehal Bhayani, Priyanka Trivedi and Megha Mohan for their support during my period of stay in Oulu.

List of abbreviations and symbols

Abbreviations

CFD	Computational fluid dynamics
VOF	Volume of fluid
RSM	Reynold stress model
LES	Large eddy simulation
DPM	Discrete phase model
NTP	Normal temperature and pressure

Latin symbols

u	Fluid velocity (m/s)
g	Gravitational acceleration (m/s^2)
P	Pressure (Pa)
k	Turbulent kinetic energy (m^2/s^2)
F_i	Body force (N/m^2)
F_vol	Volume force (N/m^2)
G_k	Production term
Q	Gas flow rate (m^3/s)
A	Area (m^2)
D	Mass diffusion coefficient (m^2/s)

Greek symbols

ρ	Density (kg/m^3)
μ	Effective viscosity (Pa.s)
μ_eff	Effective turbulent viscosity (Pa.s)
k	Turbulent kinetic energy (m^2/s^2)
ε	Turbulent dissipation rate (m^2/s^3)
μ_t	Turbulent eddy viscosity (Pa.s)
α_q	Phase volume fraction

Dimensionless number

Fr	Froude number
Co	Courant number
Sc_t	Turbulent Schmidt number

Original publications

This thesis is based on the following publications, which are referred throughout the text by their Roman numerals:

I Ramasetti, E.K., Visuri, V.-V., Sulasalmi, P., Kärnä, A., & Fabritius, T. (2017). Numerical study of multiphase flows in a ladle for different closure models. *Proceedings of the 11th Pacific Symposium on Flow Visualization and Image Processing, Kumamoto University, Kumamoto, Japan.*

II Ramasetti, E.K., Visuri, V.-V., Sulasalmi, P., & Fabritius, T. (2018). A CFD and experimental investigation of slag eye in gas stirred ladle. *Journal of Fluid Flow, Heat and Mass Transfer, 5*, 78-86.

III Ramasetti, E.K., Visuri, V.-V., Sulasalmi, P., Mattila, R., & Fabritius, T. (2019). Modeling of the effect of the gas flow rate on the fluid flow and open-eye formation in a water model of a steelmaking ladle. *Steel Research International, 90*(2), 1-15.

IV Ramasetti, E.K., Visuri, V.-V., Sulasalmi, P., Gupta, A K., Palovaara, T., & Fabritius, T. (2019). Physical and CFD modelling of the effect of top layer properties on the formation of open-eye in gas-stirred ladles with single and dual-plugs. *Steel Research International, 1900088,* 1-13.

V Ramasetti, E.K., Visuri, V.-V., Sulasalmi, P., Savolainen, J., Li, M., Shao, L., & Fabritius, T. (2019). Numerical modelling of the influence of argon flow rate and slag layer height on open-eye formation in a 150-ton steelmaking ladle. *Metals, 9(10),* 1048.

VI Ramasetti, E.K., Visuri, V.-V., Sulasalmi, P., Fabritius, T., Saatio, T., Li, M., & Shao, L., (2019). Numerical modeling of open-eye formation and mixing time in argon stirred industrial ladle. *Metals, 9(8),* 829.

All the publications were written by the author of this thesis with the help of co-authors. The author's main responsibilities were to perform experimental measurements and development of mathematical models, carrying out the calculations, reporting the results. The discussions in the articles were written with the co-authors.

Contents

Abstract
Tiivistelmä
Acknowledgements **9**
List of abbreviations and symbols **11**
Original publications **13**
Contents **15**
1 Introduction **17**
1.1 The gas stirring process in secondary metallurgy 17
1.2 Objective of the work 18
2 Literature section **21**
2.1 Modelling of two-phase flows in gas-stirred ladles 21
2.2 Modelling of the fluid flow and open eye formation in water model of a steelmaking ladle 23
2.3 Modelling of the fluid flow and open-eye formation in an industrial scale ladle 26
2.4 Mixing and homogenization in the ladle 29
3 Experimental and numerical methods **33**
3.1 Description of the experimental procedure 33
3.1.1 Experimental procedure for a water model 33
3.1.2 Experimental procedure for an industrial scale ladle 35
3.2 Description of numerical models 36
3.2.1 Conservation equations 36
3.2.2 Turbulence models 37
3.2.3 The volume of fluid model 38
3.2.4 Species transport model 39
3.3 Mesh and numerical modelling studies 39
3.3.1 Water model 39
3.3.2 Industrial scale model 42
4 Results and Discussion **45**
4.1 Verification and validation of the model developed with the data available from literature 45
4.2 Open-eye formation in the water model with different operating parameters 47
4.2.1 The effect of the gas flow rate on the open-eye formation in a single and dual-plug configuration 48

4.2.2 The effect of the top layer thickness on the open-eye formation in a single and dual-plug configuration 55
4.3 Open-eye formation in an industrial scale ladle for different operating parameters 63
4.3.1 The effect of the gas flow rate on the open-eye formation 63
4.3.2 Comparison of open-eye area with different gas flow rates and slag layer thickness 68
4.4 Mixing time distribution in industrial scale ladle 70
5 Conclusions and future work **77**
List of references **79**
Original publications **85**

1 Introduction

1.1 The gas stirring process in secondary metallurgy

In the secondary metallurgy of steelmaking, gas stirring is extensively employed to attain a homogenous distribution of alloying elements and temperature of the bath. It is employed for the process of deoxidation, desulphurization and removal of inclusions, and it intensifies the rate of reactions. Argon gas is injected through a nozzle located at the bottom of the ladle and this breaks up and forms gas bubbles. The rising bubbles tend to move upwards, forming a turbulent plume, and subsequently, a circulatory movement of the steel within the ladle. This reduces the time required to homogenise the chemical composition of alloying elements and the temperature. Meanwhile, at sufficiently high flow rates, the bubbles moving upwards break the slag layer forming an open-eye, as shown in Figure 1.

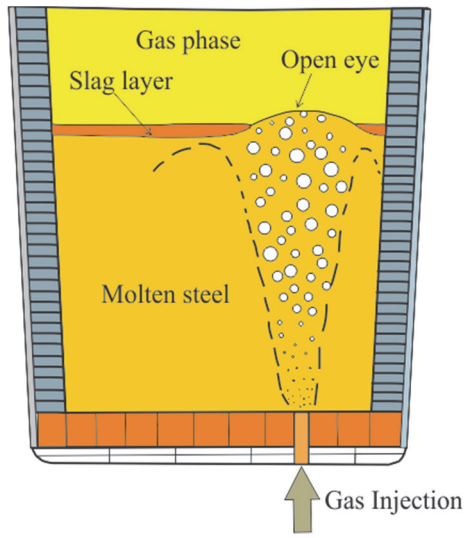

Fig. 1. Schematic illustration of the gas stirring process in the ladle (Reprinted by permission from Paper IV © 2019 Verlag GmbH & Co. KGaA).

The evolution of the open-eye process is important in ladle metallurgy because the rate of the refining reactions between the liquid steel and slag occur at the slag-steel interface. In the production of high-quality steel, it is important to understand the

fluid flow and slag-steel interface behaviour for corresponding flow rates during the refining process. The mixing behaviour, which determines the time required for the alloying elements to homogenise also depends on the flow rates. During the gas stirring process, while the gas flow rate is low and not strong enough to break the slag layer, benefits the inclusion flotation, as the open-eye formation doesn't takes place. However, the efficiency of the desulphurisation process depends on the strong interaction between slag and steel, which is possible by injecting gas with high flow rates. In addition, an appropriate open-eye area is required for the addition of desulfurizer and alloying material to improve the slag/steel intermixing. On the other hand, the formation of very large open-eye areas results in the absorption of oxygen and nitrogen from atmosphere into the liquid steel, and possibly slag entrapment into liquid steel as well. Therefore, an understanding of the formation of the open-eye and the slag layer behaviour for different gas flow rates, numbers of nozzles and slag layer heights is very important.

1.2 Objective of the work

The main objective of this thesis is to study the effect of different operating parameters on the open-eye formation process in a gas-stirred ladle. To this end, computational fluid dynamics (CFD) simulations were carried out. The simulation results were validated against data obtained from physical modelling and industrial experiments.

The aims of this work are subdivided into four task shown below:

1. To develop a CFD model for a gas-stirred ladle system and validate it with experimental data available from the literature.
2. To build an experimental setup for a 1/5 scale water model of a 150-ton industrial ladle and perform measurements for studying the effect of different operating parameters on the open-eye formation.
3. To perform CFD simulations for a water model ladle and validate them with experimental measurements.
4. To perform CFD simulations for a steelmaking ladle to study the effect of the gas flow rate on the size and mixing behaviour and validate them with industrial measurements from a steelmaking ladle.

The contents of this thesis are defined by the aims of the work and their realization. In Paper I, the CFD model for the gas-stirred ladle is developed and the simulations are validated against experimental results available in the literature. In Papers II,

III and IV, the CFD model is developed using the VOF approach to study the effect of different operating parameters on the open-eye formation in the water model. The physical model is built for the validation of the simulation results. In Paper V, the developed model is extended to investigate the effect of the gas flow rate and slag layer thickness on the open-eye formation in the industrial ladle. In Paper VI, the effect of the gas flow rate on the mixing phenomena in an industrial ladle is studied.

The role of original papers is presented in Table 1.

Table 1. The original papers content.

Paper	Contents
I	Verification of the simulation results of gas hold-up and velocity fields in the ladle with the experimental data available from the literature.
II	A study of the effect of the gas flow rate on the size in a water model ladle through experiments and simulations with a single plug system.
III	The effect of gas flow rate and number of nozzles on the open-eye size and flow field distribution is investigated through experiments and simulations.
IV	The effect of top layer thickness and density on the open-eye size in a single and dual-plug system is studied through experiments and simulations.
V	The developed CFD model is used to investigate the effect of the gas flow rate and slag layer thickness on an industrial scale ladle. The simulation results are validated with industrial measurements.
VI	A study of the effect of the gas flow rate on the mixing time of alloying elements in an industrial scale ladle.

The thesis first presents some literature research on studies related to modelling of fluid flow and open-eye formation in a water model through experiments and CFD modelling in order to provide some background to the work and to view it from a larger perspective. Then the studies related to industrial scale models through industrial measurements and CFD models are explained. The simulation results in all cases are validated with experimental data and industrial measurements.

2 Literature section

2.1 Modelling of two-phase flows in gas-stirred ladles

The studies related to describing two-phase flow phenomena in a gas-stirred system are discussed in this section.

Szekely, Wang and Kiser [1] carried out experiments and numerical simulations for a water model of an argon-stirred ladle system. The simulation was performed by solving turbulent Navier-Stokes equations and were based on using Spalding's k-ε turbulent model. The results showed good agreement of flow velocity and gas fractions when compared to the experimental measurements. A similar kind of work was also done by Ilegbusi et al. [2] investigating the flow velocities in a water model of an argon gas-stirred ladle through experiments and simulations. The simulation results were compared for two different turbulent models (k-ε and anisotropic eddy viscosity model). The predicted simulation results of the mean velocity and turbulent parameters were compared to experimental measurements.

Xie and Oeters [3] and Xie, Orsten and Oeters [4] carried out experimental measurements to investigate the flow velocity in a ladle with liquid Wood's metal with nitrogen gas injected through centric blowing. The liquid flow field was measured using magnetic probes for various blowing conditions. Measurements were taken for the bubble behaviour, as well as the local gas fraction and the rising velocity of gas bubbles for different gas flow rates and nozzle diameters. The results were presented in the form of axial and radial velocities, the gas volume fraction and the turbulent kinetic energy at different heights of the ladle. The results showed that the flow is axially symmetric when gas was blown through a nozzle at a centric location. The flow velocity on the vessel axis was almost constant over the height and increased with an increasing gas flow rate and the nozzle diameter did not influence the flow velocity in the ladle.

Xia, Ahokainen and Holappa [5] carried out numerical simulations and validated the experimental measurements an axial and radial velocity profiles of Xie and Oeters [3], and Xie, Orsten and Oeters [4]. An Euler-Euler multi-phase model was used to describe the air and water phase in the ladle. Drag, lift and turbulent dispersion forces were used describe the momentum exchange between the two phases. The simulation results showed that the developed model provided an acceptable prediction of the fluid flow in the liquid region and a relatively large

deviation in the gas-liquid plume. To describe two-phase flow phenomena in a gas-stirred system for steel making Lou and Zhu [6] studied the influence of the turbulent dispersion force, as well as drag and lift forces on the liquid flow velocity, gas fraction and turbulent kinetic energy. The mathematical model developed was based on the Eulerian approach and the simulation results were compared to experimental results.

Mendez, Nigro and Cardona [7] performed a numerical simulation to study the effects of non-drag forces (virtual mass, lift and turbulent dispersion forces) on the gas fraction and liquid flow velocities in the ladle. An Eulerian modelling approach was used by Turkoglu and Farouk [8] to investigate the liquid flow velocity, gas fraction and temperature fields in a cylindrical ladle through bottom air injection. The turbulence in the liquid phase was modelled using a two-equation k-ε turbulence model. The simulation results of the radial distribution of gas volume fraction and velocity measurements at specific axial locations were compared with experimental measurements available in the literature. The simulation results agreed well with the experimental results.

Davidson [9] conducted numerical simulations to investigate the magnitude of bubble rise velocity, centreline void fraction and the central plume in a liquid bath where gas was injected from the bottom. Domgin, Gardin and Brunet [10] carried out a detailed experimental and numerical study to investigate the mean velocity distribution and turbulent kinetic energy in a cylindrical steel bath where gas was injected through the bottom. The numerical simulations were performed based on Euler-Euler and Euler-Lagrange approaches. The simulations results of mean velocity profiles using the Euler-Euler approach were in good agreement compared to the Euler-Lagrangian approach when compared to with experimental results. A study of two different turbulence-modelling approaches (k-ε and RSM) was conducted by Park and Yang [11] for a gas stirred ladle system. The investigations included the flow velocities, gas fraction and turbulent kinetic energies. The results showed that the k-ε turbulence model was not suitable for predicting highly swirling flows, even though it yielded results that were in agreement with measurements in less swirling flows. The results also showed that the turbulent kinetic energies predicted by the k-ε model were higher than those predicted by the Reynolds stress model.

Recently Liu et al. [12] reviewed the research work carried out over a few decades into gas stirring in ladle metallurgy. This work presented the complete physical modelling and numerical simulations for four major areas: (1) mixing and homogenization in the ladle, (2) gas bubble formation, transformation, and

interaction in the plume zone; (3) inclusion behaviour at the steel-slag interface and molten steel; and (4) formation. They concluded that the mathematical models focusing on inclusion behaviour at the steel-slag interface needed to be improved.

2.2 Modelling of the fluid flow and open eye formation in water model of a steelmaking ladle

Studies related to open-eye formation in a water model ladle through physical modelling [13-22] and numerical simulations [25-33] have been performed extensively in the past three decades.

Yonezawa and Schwerdtfeger [13-15] carried out cold model measurements to investigate the open-eye size in a ladle using mercury and silicone oil to represent liquid metal and slag. The results concluded that the open-eye increased with an increase in the gas flow rate. A non-dimensional correlation was developed to represent the time-averaged open-eye size area. They also performed measurements to study the dynamics of spouts of gas plumes in a large-scale water model. In their work, a non-dimensional height, which is independent of the Froude number and nozzle diameter, was defined.

Based on the experimental data by Yonezawa and Schwerdtfeger [13-15], Krishnapisharody and Irons [16] proposed a model for estimating the plume eye area, which expresses the dimensionless eye area in terms of a density ratio of the fluids and Froude number shown in Equation (1).

$$A^* = \frac{A_e}{H^2} = \alpha + \beta \left(\frac{\rho}{\Delta\rho}\right)^{1/2} (Fr)^{1/2}, \quad (1)$$

where, α and β are numerical constants, A^* is the non-dimensional eye area, A_e is the open-eye area, H is height of the ladle, ρ is the density of water, $\Delta\rho$ is the density difference between water and oil, and Fr is the Froude number.

Krishnapisharody and Irons [17] further extended this model, developed a new one to predict the open-eye size from the primary operating variables of the ladle, and demonstrated its reliable predictive ability in a variety of multi-phase systems shown in Equation (2).

$$\frac{A_e^*}{A_p^*} = \alpha + \beta\,(1-\rho^*)^{-1/2}(Q^*)^{1/3}\left(\frac{H}{h}\right)^{1/2} \quad (2)$$

where $A_{\mathrm{e}}^* = \frac{A_{\mathrm{e}}}{H^2}$ (A_{e} is the non-dimensional open-eye area and H is the bath height), $A_{\mathrm{p}}^* = 1.41\,(Q^*)^{0.4}$,$Q^* = \frac{Q}{g^{0.5}H^{2.5}}$ (g is the gravitational acceleration), $\rho^* = \frac{\rho_{\mathrm{u}}}{\rho_{\mathrm{l}}}$ (ρ_{u} is the density of the top layer and ρ_l is the density of the water), h is the height of the top layer).

The experimental studies that Krishnapisharody and Irons [16-17] performed in a cylindrical water model ladle concluded that the open-eye area increased with increasing the gas flow rates in all cases and decreased when the top phase thickness increased. An increase in the size of the open-eye with the increasing height of the water bath was also predicted from the results, although the enlargement is not linear. To study the effect of slag (oil) properties, three liquid-liquid systems were used: (1) a water-paraffin oil system; (2) an aqueous $CaCl_2$ solution-paraffin oil system; (3) water-heavy motor oil. The results showed that the systems with less dense top phase systems had smaller s than denser top phase systems.

Wu, Valentin and Sichen [18] studied the open-eye formation in an argon stirred ladle using two physical models. To simulate liquid steel, water was used in both models. To simulate the slag, silicon oil was used in the first model and a Ga-In-Sn alloy was used in the second model. The results showed that the open-eye size highly depends on the gas flow rate, the height of the lower liquid and the height of the top liquid. In contrast, the viscosity of the top liquid and interfacial tension between the two liquids has only a slight effect on the open-eye size. Similar work was carried out by Thuman et al. [19] where they used Ga–In–Sn alloy with a melting temperature of 283 K (10 °C) to simulate liquid steel and an $MGCL_2$-glycerol (87%) solution to simulate the slag. It was found that no open-eye formed at lower flow rates, but that it did occur when the gas flow reached a critical rate. The critical flow rates were in the range of 0.7 to 4.0 NL/min and were found to depend greatly on the height of the top liquid.

Amaro-Villeda, Ramirez-Argaez and Conejo [20] studied the effect of the slag thickness on the open-eye area and the mixing time in the water model ladle. The slag thickness was varied in order to study its effect on the open-eye area and mixing time in a single plug system with a constant flow rate. A decrement of the open-eye area with an increase in slag thickness was observed. Maruyama and Iguchi [21] also performed cold model experiments in cylindrical vessel with a

mercury-silicon oil system to study the effect of slag properties on the open-eye area. The results showed that the open-eye decreases with increases in the slag thickness and the density of the slag has effect on the open-eye size only when the thickness of slag exceeds a critical value. Mazumdar, Dhandpani and Saravanakumar [22] carried out experiments to measure the open-eye area in two different water models with a gas injection nozzle located at the mid bath radius position. Liu, Li and Li [23] performed measurements in a water model for studying the formation of the open-eye with different gas flow rates, slag layer thicknesses and number of nozzles. The results showed that the open-eye area increases approximately linearly as the gas flow rate increases. The open-eye area increases quickly with a reduction in the slag layer thickness showing that the slag layer thickness has a great influence on the open-eye area.

Several mathematical models have been developed to study the flow in the ladle. Li, Liu and Li [24] developed a mathematical model by using a multiphase volume of fluid (VOF) method coupled with a population balance model (PBM) to investigate the effect of the gas flow rate and plug radial position on the gas bubble diameter, and the open-eye size in the ladle. The open-eye size predicted by the numerical model agreed well with the experimental results and a critical gas flow rate to form a steady open-eye was found for the present water mode condition. Li et al. [25] developed a mathematical model based on large eddy simulations (LES) coupled with discrete particle modelling (DPM) and a VOF model to investigate the bubble movement and slag layer behaviour during the gas stirring process in the ladle. In this approach, a VOF model was used to track the liquid-slag-air interface and the Lagrangian DPM was used for describing the bubble movement. The simulation results showed that the bubbles were found to be moving in curved paths and that they induced many eddies in the region near the bubble plume. The shape and size of the open-eye was found to be irregular. At low flow rates, the open-eye formed and collapsed alternately and at high flow rates, the slag layer fluctuated and an open-eye was formed. The predicted simulation results of the formation and closing of the open-eye qualitatively agreed with the experimental results from the water model. Li and Li [26] further extended the model developed by Li et al. [25] to investigate the bubble transport, bubble diameter redistribution, slag layer fluctuation and slag droplet generation in the water model ladle.

Calderon-Hurtadao et al. [27] performed both experiments and simulations to investigate the open-eye formation for different gas flow rates and slag layer thicknesses. For the experimental measurements, a velocity probe was placed close to the interface to monitor any turbulence. The results showed that the open-eye

was found to be strongly dependent on the gas flow rate and slag layer thickness. Liu et al. [28] and Li, Li and Liu [29] investigated the effect of the gas flow rate and oil layer on the size, bubble movement and mixing time in a water model ladle through both physical and numerical modelling. The effect of the oil layer thickness was investigated by varying it from 20 to 40 mm and 50 mm for a constant flow rate in single-plug-stirred system. The results showed the oil thickness has a large influence on the open-eye area. The open-eye area increases quickly when the oil thickness decreases and vice-versa, although the increment is not linear.

Lv et al. [30] performed numerical simulations for a cold-water model, where water and sodium tungstate were employed to simulate liquid steel, and silicon oil was employed to simulate slag. The simulation results showed that the gas flow rate, bath height and slag layer thickness had strong effects on the open-eye size. Mazumdar and Guthrie [31-33], Mazumdar, Yadhav and Mahato [34], Mazumdar and Evans [35], Mandal, Madan and Mazumdhar[36], Peranadhanthan and Mazumdhar [37], Madan, Satish and Mazumdhar [38], Patil et al. [39], Subagyo, Brooks and Irons [40] and Guo, Gu and Irons [41] contributed to a greater extent towards investigating the fluid flow analysis and open-eye formation in the ladle. Furthermore, the work also extended to developing mathematical models to investigate the mixing time in ladles.

2.3 Modelling of the fluid flow and open-eye formation in an industrial scale ladle

For industrial scale ladles, there are fewer experimental measurements for the open-eye formation available in the literature when the compared to water model ladle. This is due to the difficult conditions (e.g. high temperatures, process gases and dust) on the ladle surface, which make it quite hard to capture the process with a video camera.

Valentin et al. [42] captured the open-eye formation process in a 170-ton steelmaking ladle. The measurements included studying the effect of the stirring rate on the formation in the ladle. The trials were carried out by increasing the gas flow rate from 0 to 35 STP m^3/h (583 SLM). At a flow rate of 15 STP m^3/h (250 SLM), a circular shaped open-eye was generated approximately after two minutes of gas injection, shown in Figure 2. An increase of the flow rate to 25 STP m^3/h (417 SLM) resulted in the formation of larger open-eyes and the change of the shape from circular to oval. A further increase of the flow rate to 35 STP m^3/h (583 SLM) resulted in the formation of strong movements and turbulence on the surface

and in the top slag as well as splashing and smoke formation. During the stirring process, circulating waves were detected on the surface at higher gas flow rates. Furthermore, numerical simulations were carried out to study the flow patterns for different gas flow rates.

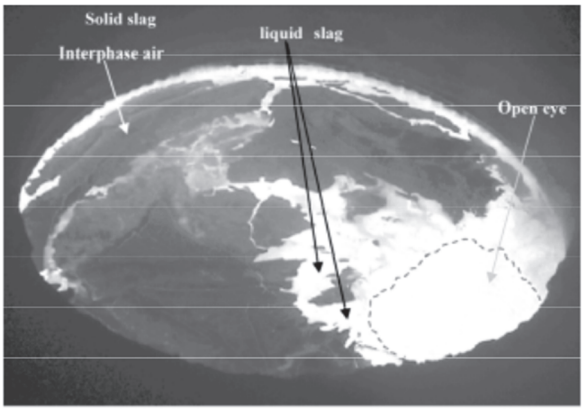

Fig. 2. Open-eye formation in a 170-ton industrial scale ladle at 15 STP m^3/h (250 SLM) from the measurements by Valentin et al. [42]. (Reprinted by permission from [42] 2009 © Wiley-VCH Verlag GmbH & Co. KGaA)

Liu, Qi and Xu [43] numerically investigated a quasi-steady fluid flow and interfacial behaviour on the industrial scale ladle with argon gas injection through one plug, and two plugs placed in 180^0 and 90^0 configurations, respectively. A VOF model was used to track the slag/steel/gas interface behaviour. The simulations were performed by increasing the flow rates from 50 to 400 L/min. The results showed that the bubble plume was not able to break the slag layer for a gas flow rate of 50 L/min. A small open-eye occurred when the flow rate was increased to 150 L/min and the open-eye size enlarged with an increase of the flow rate to 500 L/min. At high flow rates, the thickness of the slag layer became very thin near the sidewall of the ladle indicating a strong flow in the molten steel, which could damage the ladle wall refractory and reduce the ladle life. The results also concluded that the flow pattern of the molten steel was dependent on the plug configurations and gas flow rates. To avoid significant deformation of the slag layer, it was suggested to divide the gas flow into two weakened plumes by using a dual

plug configuration. For a better refining process, the proper selection of the gas flow rate and plug configurations were proposed.

Li et al. [44] developed a mathematical model to analyse the transient three-dimensional and three-phase flow in an argon stirred ladle with one and two off-centred, porous plugs. Simulations were performed on a 220-ton industrial scale ladle, increasing the gas flow rates from 100 to 300 NL/min. The simulation results showed that the injected flow rate of argon gas had a significant effect on the spout peak height and the open-eye area. The diameter of the open-eye changed from 0.43 m to 0.81 m when the flow rate of argon gas varied from 100 to 300 NL/min. When argon gas was injected through two-plugs for a flow rate of 300 NL/min, two open-eyes were generated with diameters of about 0.6 m. As concluded by Liu, Qi and Xu [43], the simulation results by Li et al. [44] also resulted in significant deformation of the slag layer during the stirring operation, and the slag thickness became thinner near the slag eye and thicker near the wall.

Singh et al. [45] developed a mathematical model to analyse a transient three-phase flow in an industrial scale ladle with argon gas injecting from off-centred plugs. The VOF model, which was used by Liu, Qi and Xu [43] and Li et al. [44] was also used in this work to track the behaviour of the slag, steel and argon gas interfaces. At first, the simulation results of the open-eye area for different operating parameters were validated with the results by Liu, Qi and Xu [43]. The results showed that the open-eye area is very much dependent on the argon-stirring rate and slag layer thickness. Furthermore, the model predicted the desulfurization rate using chemical kinetic equations, as well as the interfacial area calculated from the CFD, and thermodynamic data obtained from the Thermo-Calc software. The results demonstrated that dual-plug configurations are more suitable for larger open-eye areas, which are needed for desulfurization, than the single plug configuration.

Gonzalez et al. [46] performed numerical simulations to study the flow pattern and open-eye formation in a steelmaking ladle under non-isothermal conditions. The results of thermal stratification and velocity fields were plotted on two vertical planes. The shape of the thermal stratification layers depends on the holding time owing to convective movement of steel according to the density difference. The flow field in the ladle reached a quasi-steady state condition after 20 seconds of argon gas injection.

Cloete, Eksteen and Bradshaw [47] also developed a full-scale, three-dimensional, transient mathematical model to study the fluid flow analysis in industrial scale ladles. The Lagrangian discrete phase model (DPM) was used to

describe the bubble plume and the Eulerian VOF model for tracking the slag/steel/gas interface behaviour. The standard $k-\varepsilon$ model was used for modelling the turbulence. The results concluded that the model developed was computationally efficient for investigating the influence of a large number of operating and design variables on the fluid flow analysis and open-eye formation in the ladle. Cloete, Eksteen and Bradshaw [48] further extended this model to study the effect of plug arrangement on the flow analysis in the ladle.

Cao and Nastac [49] numerically investigated the fluid flow, mass transfer and slag-steel interface behaviour in a steelmaking ladle. In the first step, an Euler-Euler model was used to simulate the multi-phase flow in a water model and the results were validated with experimental results available from the literature. The Euler-Lagrange approach was used to study the effect of the free surface setup, injected bubble size, gas flow rate, and slag layer thickness on the slag-steel interaction and mass transfer behaviour. The argon gas floating process and open-eye formation process was investigated using both the VOF and DPM model. The gas rising upwards in the VOF model was continuous and concentrated and in the DPM model, the floating gas bubbles were dispersive and random. The decrement of the slag layer thickness resulted in the reduction in open-eye area and mass transfer coefficient in the molten steel. When the gas flow rate was increased, the mass transfer coefficient and volumetric mass transfer coefficient in the molten steel became larger, and the open-eye area enlarged. Increase in the bubble size resulted in turbulence in the ladle becoming weaker and consequently the mass transfer coefficient in steel was reduced. Cao and Nastac [50] also modelled the transport and removal of inclusions in an industrial gas-stirred ladle. The effect of the gas flow rate, injected bubble diameters and the inclusion size on various removal mechanisms including slag capture, bubble attachment and ladle wall adhesion on the removal of inclusions was investigated.

2.4 Mixing and homogenization in the ladle

The studies related to describing the mixing phenomena in a water model and steelmaking ladle are discussed in this section.

Palovaara, Visuri and Fabritius [51] performed physical modelling measurements in a 1:5 scale water model of a 150-ton ladle to study the effect of the gas flow rate on the mixing phenomena. The mixing time was determined based on the change of the pH of the water bath using sulphuric acid as a tracer substance. The results indicated that the average mixing time decreases with increases in the

gas flow rate non-linearly. Michaelek, Gryc and Moravka [52] studied the mixing phenomena through physical modelling in 1:10 scale water model. The mixing time was evaluated based on electrical conductivity and temperature changes, which were measured at three points in the ladle. The results obtained illustrated that the time required for homogenization decreased with an increase in the gas flow rate. Joo and Guthrie [53] investigated the mixing behaviour and mixing mechanisms as a function of the location of a porous plug, the tracer injection point, and ladle monitoring point. From the results, it was shown that eccentric bubbling gives steady results in terms of reducing the mixing times, since an angular momentum intermixes fluid across the width of the ladle.

Terrazas and Conejo [54] investigated mixing phenomena in a water model ladle. The measurements included studying the effect of process variables such as the nozzle diameter, gas flow rate and nozzle radial position on the mixing time. The mixing time decreased with an increase the nozzle diameter at low stirring rates, but at high stirring rates this effect was found to be relatively significant. The nozzle plug location played a pivotal role in the mixing time, and it is found that there is was a large decrement in the mixing time when the radial position of the nozzle was changed from the centre of the ladle to a half radius position (i.e. to an eccentric position).

Conejo et al. [55] studied the effect of the top layer, nozzle arrangement, number of nozzles and gas flow rate on the mixing time in a 1:18 scale water model. The experimental results suggested that one nozzle located eccentrically at a distance of 0.67 R, with no slag, results in a shorter mixing time in comparison to two nozzles with separation angles of 180, 120, and 60 degrees, located at any radial distance. The mixing time decreased at low gas flow rates and increased at high gas flow rates, and in some cases, the slag layer thickness promoted a decrease in the mixing time.

Pan, Chaing and Hwang [56] investigated the effects of injection conditions on the mixing efficiency of the gas injection treatment in a water model. The results of these measurements concluded that the mixing efficiency was improved with increments of the gas flow rate and that an off-centre injection was better than centreline injection. Aoki et al. [57] investigated mixing phenomena in a bottom gas-stirred ladle through experiments and theoretical studies. Liu, Li and Li [23] studied the effect of gas flow rates and the number of porous plugs on the mixing time in a water model through physical modelling measurements.

Cao and Nastac [58] developed three-dimensional DPM-VOF coupled model to study the mixing phenomena in the industrial scale ladle. From the simulation

results, it was found that two symmetrical plugs configuration provides higher mixing efficiency in the ladle when compared to one centric or one eccentric plug configuration. Lou and Zhu [59] developed a coupled model based computational fluid dynamics and population balance model (CFD-PBM) to investigate the effects of different numbers and positions of the nozzles, and the gas flow rate on the mixing phenomena in the 150-ton steelmaking ladle. The simulation results revealed that dual blowing gives a shorter mixing time in comparison to centric blowing configurations. The mixing time decreases with increase in the gas flow rate, and when the gas glow rate exceeds 300 NL/min the change in mixing time is small.

Geng, Lei and He [60] developed a mathematical model based on a two-phase fluid (Eulerian-Eulerian) to investigate the effect of the offset of dual plugs and the gas flow rate on the mixing time in a ladle with dual plugs. Ramirez-Argaez [61] performed calculations to study the effect of the gas flow rate, injector position, number of injectors, and ladle geometry on the mixing time. The simulation results showed that increments in the number of porous plugs resulted in longer mixing times. Haiyan et al. [62] numerically studied the effect of the gas flow rate, number, position and relative angle of porous plugs on the mixing time in the ladle. Zhu et al. [63] performed experiments and numerical simulations to study the mixing phenomena in an argon-stirred ladle with six types of porous plug arrangements. It was found that the porous plug arrangement has a significant effect on the mixing time.

Over the past decade, there have been relatively few studies on both physical and CFD modelling together with strong validation in studying the gas-steel-slag interface behaviour in the ladle. Moreover, the studies have focused more on modelling water models when compared to the modelling industrial ladles. In the current work, the simulation results of open-eye behaviour and mixing phenomena are provided with strong experimental data measured for validation and vice-versa. As for the experimental part, the work focuses on measuring the open-eye size for different flow rates, slag layer thickness and slag layer properties (density and viscosity) in water model and industrial measurements. The industrial measurements were performed at Outokumpu Stainless Oy in Tornio, Finland. As for the simulation part, the work focused on the development of the CFD model with the VOF approach to track the slag/steel/gas interface behaviour and species transport model for calculating the mixing time in the gas-stirred ladle.

3 Experimental and numerical methods

3.1 Description of the experimental procedure

3.1.1 Experimental procedure for a water model

An industrial ladle of 150 tonnes of nominal capacity was used as a prototype to design the water model with a geometric scale factor of 1:5. Palovaara, Visuri and Fabritius [51] introduced the water model for investigating the effect of gas flow rate on the open-eye area and mixing time in the ladle. The model was used later for validating CFD simulations [Papers II, III and IV] as well as for studying the vibrations induced by gas-stirring [66]. The dimensions of the water model are presented in Table 2.

Table 2. The dimensional parameters of water model (Reprinted by permission from Paper IV © 2019 Verlag GmbH & Co. KGaA).

Parameters	Values
Diameter of the bottom of the ladle	273.3 mm
Diameter of the top of the ladle	298.8 mm
Height of the ladle	755 mm
Top layer thickness	7.5 to 75 mm (thickness)
Effective height filled with water	520 mm
Porous plug diameter	8 mm
Plug radial position	0.54 R

Air was injected into the water bath through plugs with a diameter of 8 mm located at the bottom of the bath. The gas injection was measured in terms of the NTP conditions (20 °C, 1 atm). The position of the plugs is presented in Figure 3.

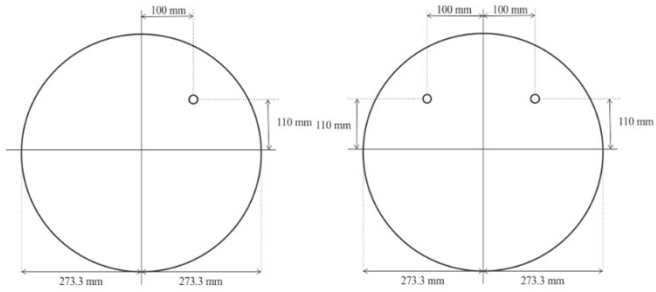

Fig. 3. Nozzle plug arrangement for single (left) and dual (right) plug systems (Reprinted by permission Paper IV © 2019 Verlag GmbH & Co. KGaA).

The water model was filled with water up to a height of 520 mm from the bottom wall. The top layer thickness varied from 7.5 mm to 75 mm in the water model to study the effect of the top layer thickness on the open-eye area. The physical modelling setup is shown in Figure 4.

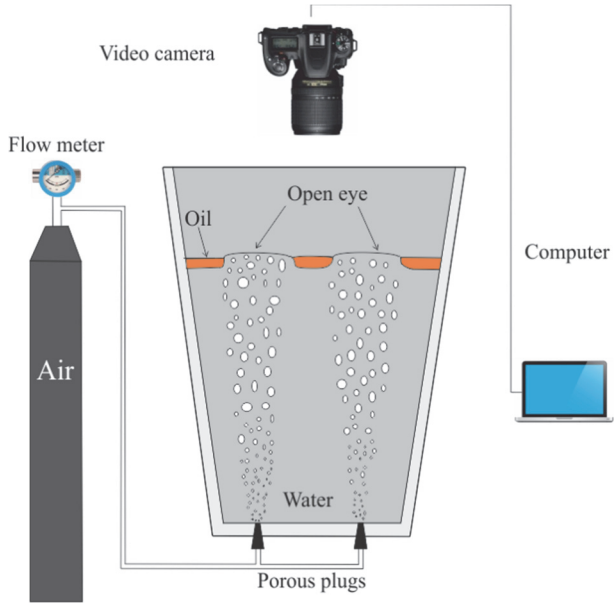

Fig. 4. Experimental setup for the water model (Reprinted by permission from Paper IV © 2019 Verlag GmbH & Co. KGaA).

To represent the liquid metal and argon gas, water and air were used, respectively. To simulate the slag, three different oils were employed: rapeseed oil, castor oil and paraffin oil. The three different oils, castor oil (denser), rapeseed oil (dense) and paraffin oil (less dense) were chosen so that the effect of the density and viscosity on the open-eye formation could be studied. Based on the colour difference between the water and oil, the movement of the open-eye was predicted by mounting a video camera perpendicular to the surface of the water bath. ImageJ software was used to determine the open-eye size by processing the recorded images taken by the camera. The measurements were taken with a top layer thickness ranging from 0.75 cm to 7.5 cm and gas flow rates varying from 1.5 to 15 NL/min. To study the effect of slag viscosities on the open-eye area, castor and paraffin oil were used to represent liquid steel. The thermal physical properties used in the physical modelling are shown in Table 3.

Table 3. Physical properties and parameters employed for the water model (Reprinted by permission from Paper IV © 2019 Verlag GmbH & Co. KGaA).

Parameters	Values	Units
Density of water	997.2	kg/m^3
Dynamic viscosity of water	0.000891	Pa·s
Density of rapeseed oil [64]	907.3	kg/m^3
Dynamic viscosity of rapeseed oil [65]	0.0778	Pa·s
Density of castor oil [64]	956	kg/m^3
Dynamic viscosity of castor oil [65]	0.57	Pa·s
Density of paraffin oil [64]	880	kg/m^3
Dynamic viscosity of paraffin oil [65]	0.06	Pa·s
Density of air (20^0C)	1.258	kg/m^3
Dynamic viscosity of air (20^0C)	1.846×10^{-5}	Pa·s
Gas flow rate	1.5 to 7.5 (varies)	NL/min

3.1.2 Experimental procedure for an industrial scale ladle

The ladle studied in this work is a 150-ton ladle owned by Outokumpu Stainless Oy in Tornio, Finland. The physical properties and operating parameters are shown in Table 4.

Table 4. Physical properties and operating parameters employed for the industrial scale ladle. (Reprinted by permission from Paper V © 2019).

Physical properties at 1812 K	Values	Units
Density of liquid steel [67]	6913	kg/m^3
Viscosity of liquid steel [67]	0.005281	Pa·s
Density of slag	2746	kg/m^3
Viscosity of slag	0.081	Pa·s
Density of argon gas	0.8739	kg/m^3
Viscosity of argon gas	2.2616×10^{-5}	Pa·s
Temperature of steel bath	1812	K
Flow rate of argon gas	200, 400 and 500	NL/min*)
Slag layer height	25, 40 and 55	cm

*) Normal temperature and pressure (NTP): 293.15 K and 101325 Pa

The experiments were conducted with gas flow rates varying from 200 to 500 NL/min and a slag layer thickness varying from 25 to 55 cm. The slag layer height in the industrial ladle was determined by measuring with a steel-rod. An IR camera from Sapotech Oy was used to monitor the open-eye formation and evolution in the industrial ladle operated at very high temperatures. ImageJ software was used to measure the open-eye size by processing the recorded images taken by the camera.

3.2 Description of numerical models

In the current work, a VOF model was used to solve the three-phase flow and to track the slag/steel/gas interface behaviour in the ladle. The following governing equations of the VOF model and turbulence model need to be solved [68].

3.2.1 Conservation equations

The continuity and momentum equations are shown in Equations (3) and (4), respectively.

Continuity equation

$$\frac{\partial \rho}{\partial t} + \frac{\partial (\rho u_i)}{\partial x_i} = 0, \tag{3}$$

Momentum equation

$$\frac{\partial(\rho u_i)}{\partial t}+\frac{\partial\left(\rho u_i u_j\right)}{\partial x_j}=-\frac{\partial p}{\partial x_i}+\frac{\partial}{\partial x_j}\left[\mu_{\text{eff}}\left(\frac{\partial u_i}{\partial x_j}+\frac{\partial u_j}{\partial x_i}\right)\right]+F_i+F_{\text{vol}}, \tag{4}$$

where F_i is the body force in the case of gas blowing in the ladle and F_{vol} is the volume force which the source term for surface tension, given by

$$F_i=\alpha\rho_l g_i, \tag{5}$$

$$F_{vol}=\sigma_{ij}\frac{\rho\kappa_i\nabla\alpha_i}{\frac{1}{2}(\rho_i+\rho_j)}, \tag{6}$$

3.2.2 Turbulence models

The standard $k-\varepsilon$ equation is used to model the turbulence, which solves two equations for the transport of turbulent kinetic energy and its dissipation rate to obtain the effective viscosity field.

$$\rho\frac{\partial k}{\partial t}+\frac{\partial(\rho k u_i)}{\partial x_i}=\frac{\partial}{\partial x_i}\left[\left(\mu+\frac{\mu_{\text{t}}}{\sigma_{\text{k}}}\right)\frac{\partial k}{\partial x_i}\right]+G_k-\rho\varepsilon, \tag{7}$$

$$\rho\frac{\partial\varepsilon}{\partial t}+\frac{\partial(\rho\varepsilon u_i)}{\partial x_i}=\frac{\partial}{\partial x_i}\left[\left(\mu+\frac{\mu_{\text{t}}}{\sigma_{\varepsilon}}\right)\frac{\partial\varepsilon}{\partial x_i}\right]+C_{1\varepsilon}\frac{\varepsilon}{k}(G_{\text{k}}+C_{3\varepsilon}G_{\text{b}})-C_{2\varepsilon}\rho\left(\frac{\varepsilon^2}{k}\right), \tag{8}$$

where k is the turbulent kinetic energy, ε is the turbulent dissipation rate, and x_i represents the spatial coordinates for different directions. G_{k} is the turbulent kinetic energy source term caused by mean velocity gradients, and G_{b} is the turbulent kinetic energy source term caused by buoyancy. These terms are calculated by Equations (9) and (10).

$$G_k = -\rho u_i u_j \frac{\partial u_i}{\partial u_j}, \tag{9}$$

$$G_b = -g_i \left(\frac{\mu_t}{\rho} Pr_t\right) \frac{\partial \rho}{\partial x_i}, \tag{10}$$

$$\mu_t = \frac{\rho C_\mu k^2}{\varepsilon}, \tag{11}$$

The turbulent viscosity is calculated by Equation (11) using k and ε from, Equations (7) and (8) respectively. The constants k and ε used in the present study were recommended by Launder and Spalding [79].

3.2.3 The volume of fluid model

The Volume of Fluid (VOF) model can be used to track the interface between the phases by solving a single set of momentum equation. In this work, the tracking of the interfaces between liquid steel/slag/top-gas is accomplished using this model. The governing equation can be written as follows:

$$\frac{1}{\rho_q}\left[\frac{\partial}{\partial t}(\alpha_q \rho_q) + \nabla . (\alpha_q \rho_q \vec{v}_q)\right] = S_{\alpha_q} + \sum_{p=1}^{n} (\dot{m}_{pq} - \dot{m}_{qp}), \tag{12}$$

where $\dot{m}_{pq}$, $\dot{m}_{qp}$ represent the mass transfer from phase p to q and phase q to p in unit time and volume, respectively; α_q is the volume fraction of phase q, ρ_q is the density of phase q, S_{α_q} is the source term taken as 0 in the Fluent software. The volume fraction of the main phase is not calculated in the Fluent software, while it can be acquired by Equation (13). When the volume fractions are summed the following equation is satisfied:

$$\sum_{q=1}^{n} \alpha_q = 1. \tag{13}$$

3.2.4 Species transport model

To calculate the mixing process in the ladle, the species transport model was solved throughout the computational domain

$$\frac{\partial(\rho c)}{\partial t} + \nabla.(\rho u c) = \nabla.[\rho\left(D + \frac{\mu_t}{\rho \mathrm{Sc}_t}\right)\nabla c\,, \tag{14}$$

where D is the mass diffusion coefficient and Sc_t is the turbulent Schmidt number with a default value of 0.7 ($\mathrm{Sc}_t = \frac{\mu_t}{\rho D_t}$ where D_t is the turbulent diffusivity).

3.3 Mesh and numerical modelling studies

3.3.1 Water model

The computational domain and mesh

The geometry was developed according to a one-fifth scale water model. The dimensions of the geometry are reported in Table 2. A completely structured hexahedral mesh with 800,000 cells was generated; the computational mesh and boundary conditions for the model with single and double nozzles are shown in Figure 5. The three-phase transient flow simulations were performed using the Ansys Fluent 18 software. The VOF model with an explicit scheme was used to solve the volume fraction equation. The plug was approximated as a nozzle in the simulations and the diameter used was 8 mm. A no-slip boundary condition was used at the bottom wall and sidewalls. A velocity inlet boundary condition was employed for the gas inlet, and a pressure outlet boundary condition was chosen for the outlet.

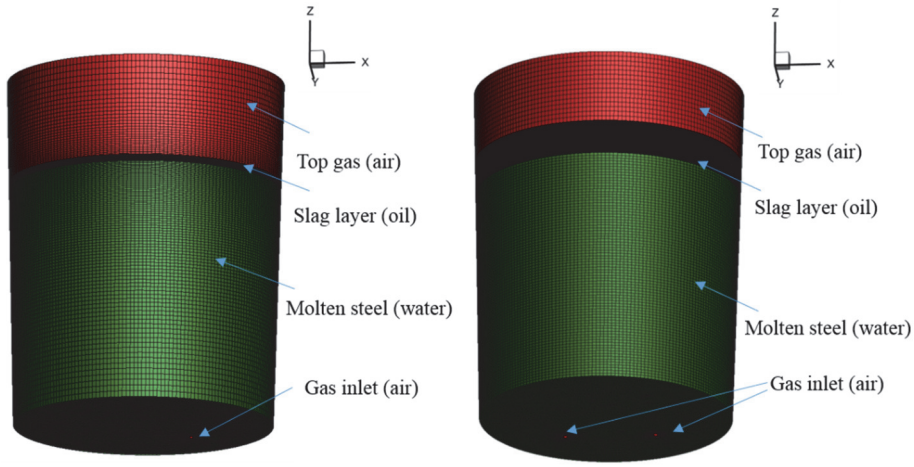

Fig. 5. The mesh distribution for the ladles for a single plug system with a top layer thickness of 0.75 cm (left) and for a dual plug system with a top layer thickness of 7.5 cm (right) (Reprinted from by permission from Paper IV © 2019 Verlag GmbH & Co. KGaA).

Grid independency test

The mesh sensitivity tests were conducted for several mesh densities with top layer height varying from 0.75 to 4.5 cm. Figure 6 shows results of the mesh independency test for the top layer height of 3.0 cm and flow rate of 5.0 NL/min. The open-eye area changed significantly with the refinement of mesh from 120,000 to 830,000. However, the accuracy of the results was not affected by further refinement of the mesh. Based on the test results, the optimum grid size was selected varying from 650,000 cells for 0.75 cm top layer height to 830,000 cells for 3.0 top layer height to 1 million cells for a 7.5 cm top layer height configurations.

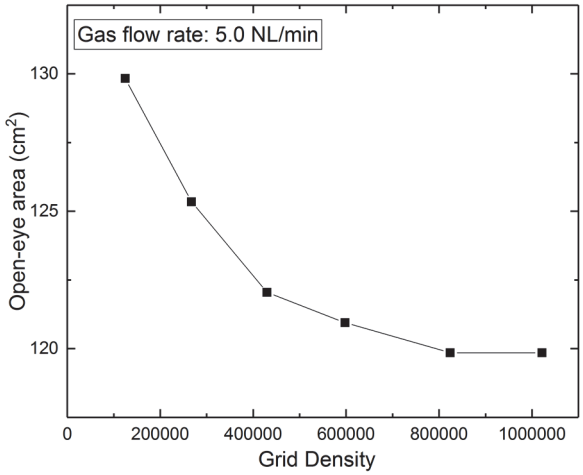

Fig. 6. Results of the grid independence tests with a top layer thickness of 3.0 cm for a single plug system. (Reprinted from by permission from Paper III © 2019 Verlag GmbH & Co. KGaA).

Initial and boundary conditions

The water model is at rest at the initial stage, with no injection of air from the bottom plug(s). Because heat transfer is not within the scope of this work, temperatures changes in the water model were ignored. The velocity inlet boundary condition of the air was calculated according to the flow rates used in the physical modelling by Equation (15).

$$v_{\text{in}} = \frac{Q_{\text{L}}}{A} = \left(\frac{p_{\text{S}}}{p_{\text{L}}}\right)\left(\frac{T_{\text{L}}}{T_{\text{S}}}\right)\frac{Q_{\text{S}}}{A}, \tag{15}$$

where, subscript 'L' means the water model operating condition, and 'S' is the standard condition. T_{S}= 293.15 K (20 °C), T_{L} = 298.15 K (25 °C), p_{S}= 1 atm (101325 Pa), and p_{L} is the total pressure at the vessel bottom. A is the bottom plug area, and Q_{S} is the air flow rate in the standard condition.

3.3.2 Industrial scale model

The computational domain and mesh

The computational mesh and boundary conditions of the industrial scale ladle configurations are shown in Figure 7. The ANSYS ICEM CFD software was used to generate a structured mesh with hexahedral elements. The mesh with approximately 1 million cells was created by setting the maximum mesh size of 8 mm throughout the domain and 4 mm for the inlet and slag layer. The simulations were carried out in ANSYS Fluent software by using the volume of fluid (VOF) model to track the interface with an explicit geo-construct scheme. The same boundary conditions as in water model discussed in the above section 3.3.1 were used for the industrial scale ladle.

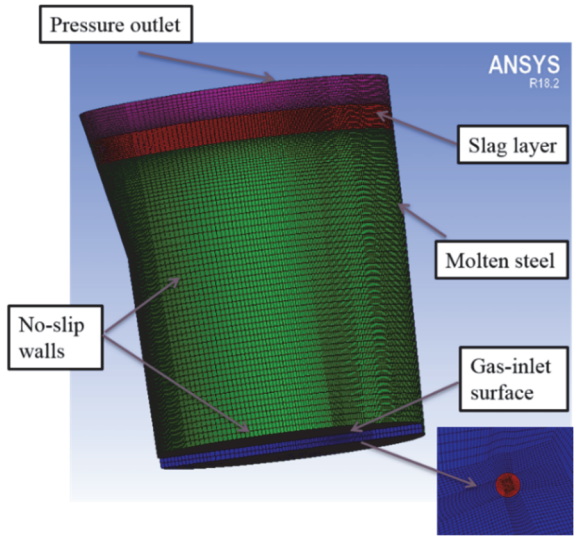

Fig. 7. The computational domain and mesh of the industrial scale ladle (Reprinted by permission from Paper V © 2019).

Initial and boundary conditions

For the industrial ladle, the temperature of the metal was assumed to be 1812 K (1539°C) based on collected experimental data. The same Equation (15), which was used to calculate the velocity inlet boundary condition for water model, was also used for the industrial ladle case by using the flow rates of argon gas:

$$v_{\text{in}} = \frac{Q_{\text{L}}}{A} = \left(\frac{p_{\text{S}}}{p_{\text{L}}}\right)\left(\frac{T_{\text{L}}}{T_{\text{S}}}\right)\frac{Q_{\text{S}}}{A}, \tag{15}$$

where subscript L is the ladle operating condition and S is the standard condition. T_{S} = 293.15 K (20 °C), T_{L} = 1812 K (1539 °C), p_{S} = 1 atm (101325 Pa), and $p_{\text{L}} = p_{\text{S}} + \rho_{\text{L}} g H$. A is the plug area, and Q_{S} is the measured argon gas flow rate at a normal temperature and pressure (NTP).

4 Results and Discussion

The main results from the original papers are summarised in this chapter. First, the results of the CFD model validation of the literature (Paper I), and then the open-eye formation in the water model ladle (Papers II– IV) are presented with a discussion. Finally, the main results of the thesis, i.e. the results of the open-eye formation and mixing times in an industrial scale ladle (Papers V & VI) are presented with some further discussion.

4.1 Verification and validation of the model developed with the data available from literature

In Paper I, the focus of the study was to carry out simulations to verify and validate the experimental results available in the literature. The experimental data of flow velocities in the ladle measured by Xie and Oeters [3] and Xie, Orsten and Oeters [4] were chosen to validate the simulation results. In this work, a mathematical model was based on an Euler-Euler approach for a two-phase gas stirred ladle. The geometry used in the simulations is identical to the ladle used by Xie and Oeters [3] and Xie, Orsten and Oeters [4] for experimental measurements. The dimensions of the geometry were 400 mm in diameter and a height of 370 mm. The ladle was filled with liquid Wood's metal and nitrogen gas was injected through a nozzle with a diameter of 3 mm located centrally at the bottom. The Schiller Naumann drag model was used to describe the drag force between the phases and a lift coefficient of 0.5 used.

The effect of flow rates on the flow velocity distribution in the ladle is displayed in the Figure 8. As seen in the Figure 8, the liquid flow velocities in the ladle is increased with the increase in the flow rate from 100 to 800 cm^3/s. Figure 9 depicts the simulation results for the liquid velocity profiles using three different turbulence models (k-ε, k-ω and Reynolds Stress Model) at four different heights. The velocity profiles very similar using k-ε and k-ω turbulence models when compared to the measured from Xie and Oeters [3] at all heights. On the other hand, the liquid velocity profiles using RSM were good agreement with the experimental data at heights 0.05 and 0.15 m and slightly higher at heights 0.25 and 0.35 m.

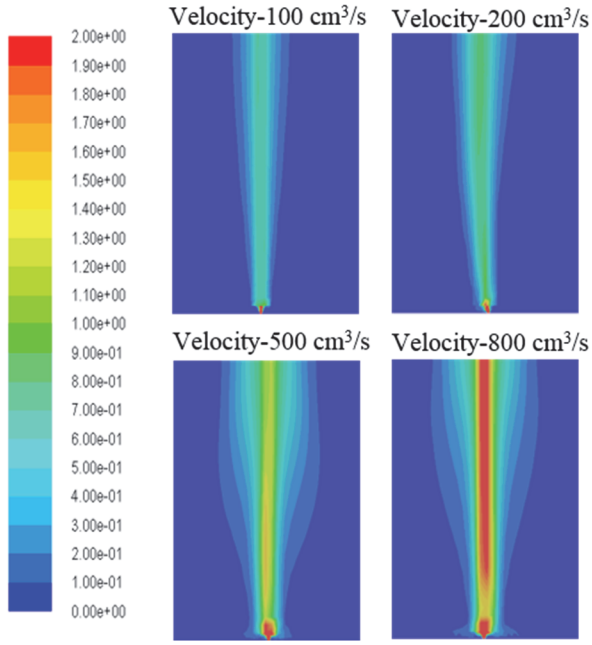

Fig. 8. Velocity filed distribution for different gas flow rates in the vertical plane section (Reprinted by permission from Paper I © 2017 The 11th Pacific Symposium on Flow Visualization and Image Processing).

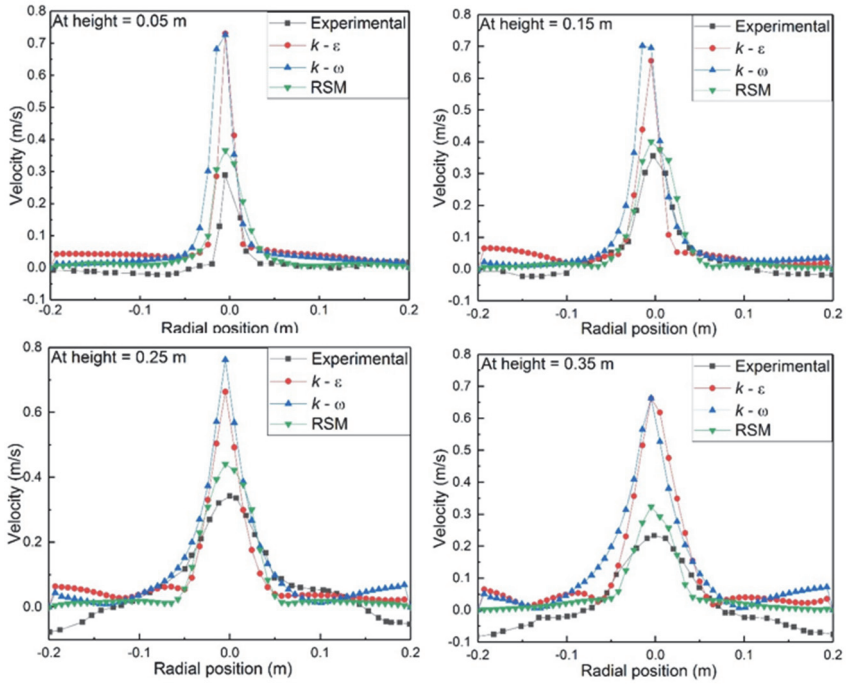

Fig. 9. A comparison of liquid flow velocity profiles at different heights in the ladle for different turbulence models to the experimental data from Xie and Oeters [3] (Reprinted by permission from Paper I © 2017 The 11th Pacific Symposium on Flow Visualization and Image Processing).

4.2 Open-eye formation in the water model with different operating parameters

In Papers II, III and IV, the focus of the study was on developing a CFD model for studying the open-eye formation in the water model. A physical model was used for validation of the CFD model. The effect of the gas flow rate, number of nozzles, top layer (slag) thickness and density on the open-eye size was studied. A 1:5 scale water model of a 150-ton industrial ladle was used for the physical modelling to obtain validation data for the CFD model. The dimensions of the water model and physical properties of the phase are presented in Table 2 and Table 3, respectively. In this study, water and rape-seed oil were used to simulate liquid steel and slag.

4.2.1 The effect of the gas flow rate on the open-eye formation in a single and dual-plug configuration

The effect of the gas flow rate on the formation in single and dual-plug configurations was studied in Papers II and III.

The effect of the gas flow rate on the open-eye formation in a single plug system

In the Paper II, the simulations were focused on studying the effect of gas flow rates ranging from 1.5 to 15 NL/min with a top layer thickness of 40 mm on the open-eye size in single plug configurations. The experimental and simulation results with the developed CFD model of the open-eye diameter presented in Paper II are shown in Table 5.

Table 5. Open-eye diameter values for different gas flow rates from the experimental and simulation results obtained in Paper II.

Gas flow rate (NL/min)	Top layer thickness (mm)	Experimental: Diameter (cm)	Simulation: Diameter (cm)
1.5	40	5.05	5.29
3.5	40	7.14	7.57
7.5	40	11.28	12.86
15.0	40	15.26	16.16

The open-eye diameter increased from 5.05 to 15.26 cm in the experiments and from 5.29 to 16.16 cm in the simulations when the gas flow rate was increased from 1.5 to 15 NL/min. The relative error between the experimental and simulated values of the open-eye diameter increased from 2.4 to 5.9% when the gas flow rate was increased from 1.5 to 15 NL/min. The work presented in Paper II represents the first step towards modelling an industrial ladle.

In Paper III further investigations were carried out by extending the developed CFD model to simulate the effect of the gas flow rate on the relative open-eye area in the single and dual plug configurations. A similar computational domain as in Paper II was applied, but a detailed study of mesh independence, steady-state conditions and additional simulations for finding the optimum flow rate for the opening of an open-eye was performed. The effect of the gas flow rate on the open-eye in the dual-plug configuration was also studied. The studied cases presented in Paper II are shown in Table 6.

Table 6. Properties of the simulated cases in Paper III.

Single plug system, top layer thickness 3.0 cm					
	Case S1	Case S2	Case S3	Case S4	Case S5
Gas flow rate (NL/min)	0.75	1.5	3.5	7.5	15
Dual-plug system, top layer thickness 3.0 cm					
	Case D1	Case D2	Case D3	Case D4	Case D5
Gas flow rate (NL/min)	0.75	1.5	3.5	7.5	15

Figures 10 to 12 present the experimental and simulation results of the effect of the gas flow rate on the open-eye size in a single plug system for cases S1, S3 and S5 at a height of 0.55 m from the bottom of the model. A small open-eye occurred when a flow rate of 0.75 NL/min was used (see Figure. 10). At a high gas flow rate of 15 NL/min, it was observed that there were significant deformation of the slag layer during gas stirring, and the thickness of the slag layer became thin near the open eye. This indicates that there would be a strong flow in the liquid metal, which may damage and reduce the life of ladle, which was also concluded by Liu, Qi and Xu [43]. When the gas flow rate was increased beyond 15 NL/min, the open-eye became highly dynamic and the fluid flow was more turbulent.

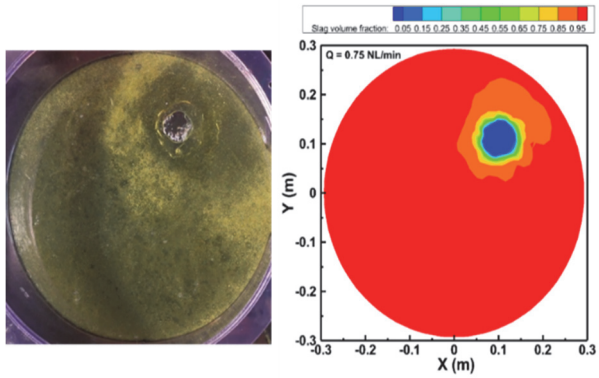

Fig. 10. The open-eye size in the physical model (left) and simulation (right) in Case S1 (Under CC-BY-NC-ND Paper III © 2018 Authors).

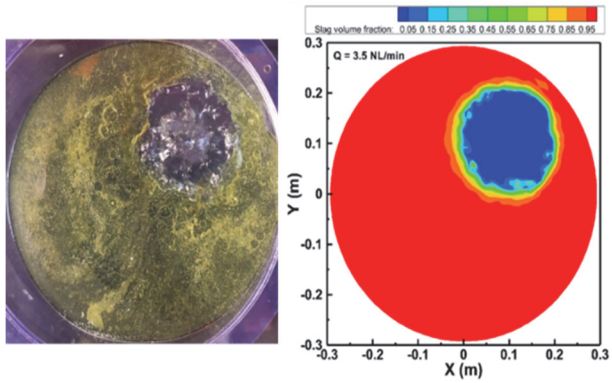

Fig. 11. The open-eye size in the physical model (left) and simulation (right) in Case S3 (Under CC-BY-NC-ND Paper III © 2018 Authors).

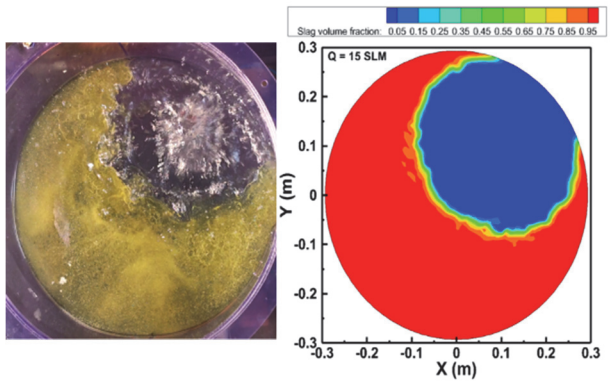

Fig. 12. The open-eye size in the physical model (left) and simulation (right) in Case S5 (Under CC-BY-NC-ND Paper III © 2018 Authors).

The effect of the gas flow rate on the open-eye formation in a dual-plug system

Figures 13 to 15 present the experimental and simulation results of the effect of the gas flow rate on the open-eye size in a dual-plug system for cases D1, D3 and D5 at a height of 0.55 m from the bottom of the model. In the dual plug system, air was injected through the two nozzles present at the bottom of the model, which results in the formation of two open-eyes.

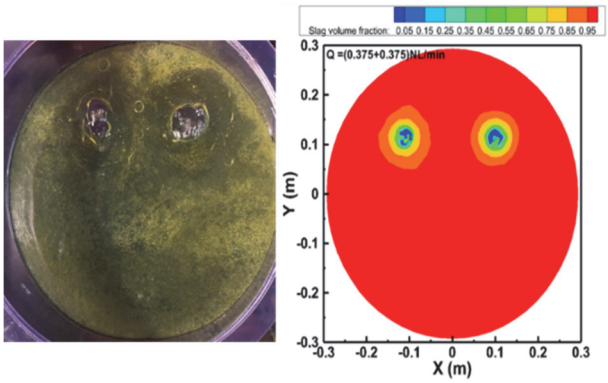

(a) (b)

Fig. 13. The open-eye size in the physical model (left) and simulation (right) in Case D1 (Under CC-BY-NC-ND Paper III © 2018 Authors).

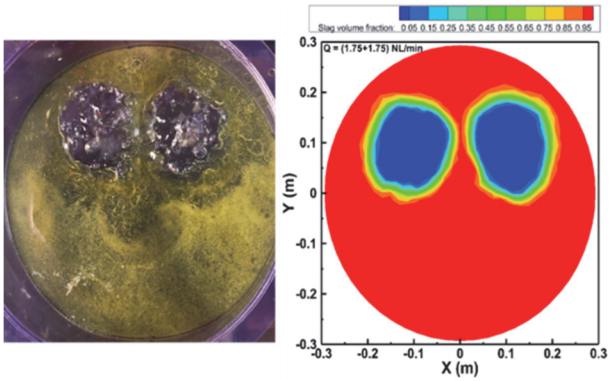

(a) (b)

Fig. 14. The open-eye size in the physical model (left) and simulation (right) in Case D3 (Under CC-BY-NC-ND Paper III © 2018 Authors).

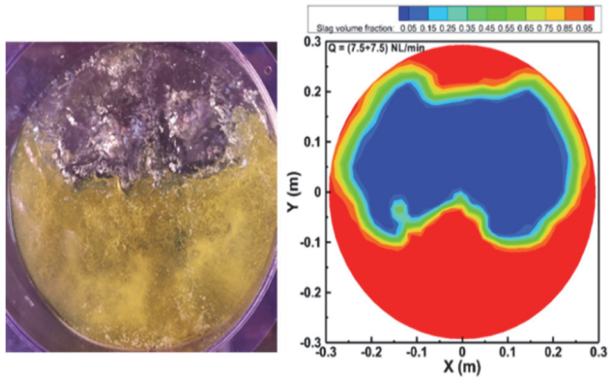

(a) (b)

Fig. 15. The open-eye size in the physical model (left) and simulation (right) in Case D5 (Under CC-BY-NC-ND Paper III © 2018 Authors).

As we can observe in Figure 13, the open-eye is quite hard to form when a gas flow rate of 0.375 NL/min was injected from both nozzles. A series of experiments was conducted to measure the critical gas flow rate as the two open-eyes started to merge into one large open-eye. When the flow rate was increased to 3.75 NL/min in each plug, the two open-eyes formed tended to merge and form the single open-eye shown, and a gas flow rate of 7.5 NL/min in both nozzles generated one large open-eye by merging the two generated open-eyes, as shown in Figure 15. This information will help to select appropriate flow rates to generate a larger open-eye for better alloying practice when using double nozzles. To avoid the deformation of the slag layer at high gas flow rates, it might be beneficial to use dual plugs by dividing the gas flow into two weakened plumes.

Comparison of the open-eye areas between single and dual-plug systems

The enlargement of the relative open-eye area with the increment in the gas flow rate in single and dual-plug systems in displayed in Figure 16.

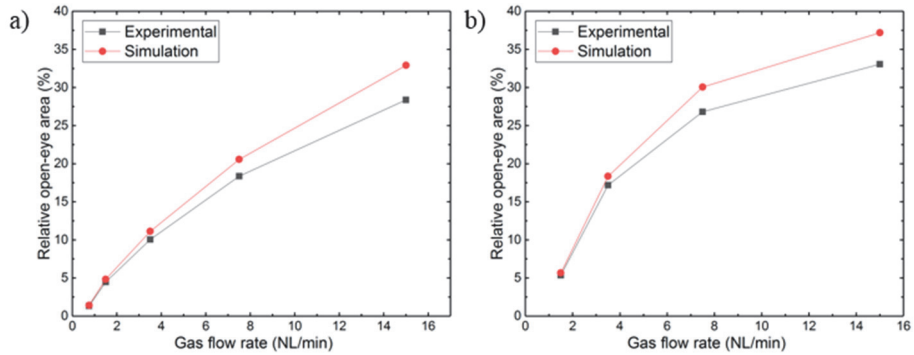

Fig. 16. Percentage of the open-eye area relative to the bath top surface area as a function of gas flow rate in a) single plug system and b) dual plug system (Under CC-BY-NC-ND Paper III © 2018 Authors).

In a single plug system, the relative open-eye area enlarged from 1.32 to 28.37% in the physical modelling and from 1.41 to 32.90% in the numerical simulations when the gas flow rate increased from 0.75 to 15.0 NL/min. In the dual plug system, the relative open areas of two open-eyes enlarged from 5.37 to 33.06% in the physical modelling and from 5.66 to 37.18% in the numerical simulations when the gas flow rate was increased from 0.75 to 7.5 NL/min in each plug. The relative error between the measurements and the simulation data is approximately 15% at high gas flow rates.

At high flow rates, the open-eye moves closer to the ladle walls increasing the flow velocities near to the ladle surface. To calculate the average flow velocity near to the ladle wall in the region near the slag-steel surface, a user defined function (UDF) was employed. Figure 17 depicts the effect of the number of plugs on the average flow velocity near the wall.

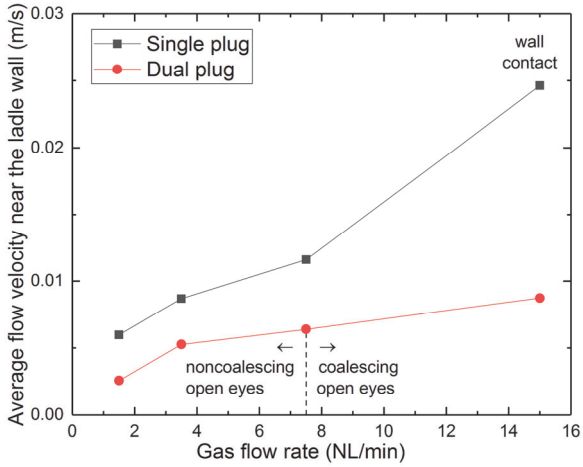

Fig. 17. The effect of the number of the plugs on the average flow velocity near the ladle wall (Under CC-BY-NC-ND Paper III © 2018 Authors).

As explained in Paper III, the average velocity near the wall is greater for a given flow rate in the one plug system when compared to the double plug system. In alloying, an open-eye is formed to avoid the contact between the alloying material and slag when the material is fed into the steel. In order to create large enough open-eye for the purpose, gas flow rate must be sufficiently high. High flow rates increase the operating expenses and, furthermore, increase the flow rates near the wall leading to mechanical wear of the refractory. When using the dual plug system, sufficiently high flow rates must be employed in order to form one open-eye instead of two separate open-eyes. With the results presented, it can be stated that with double-plug blowing a larger open-eye can be created but with slower flow at the ladle wall. Furthermore, judging from Figures 10–12 and Figures 13–15 it seems that the wall contact of the open-eye can be better avoided in the dual plug systems. From Figure 17 it can be seen that in the single plug system the wall contact at the highest flow rate results in a more intensive flow near the ladle wall. As a conclusion it can be said that, from an alloying point of view, a given volumetric gas flow rate using two bottom plugs instead of one seems to be a preferable choice because a larger open-eye can be created with a lesser mechanical wear subjected to the refractory.

4.2.2 The effect of the top layer thickness on the open-eye formation in a single and dual-plug configuration

In Paper IV, the investigations focused on studying the effect of the top layer thickness and density on the open-eye formation. The top layer thickness was increased from 0.75 to 7.5 cm for a constant flow rate of 7.5 NL/min. In order to evaluate of the effect of the top layer densities on the open-eye area, experiments were conducted using two additional oils which were chosen based on their density: castor oil (956 kg/m^3) is heavier than rapeseed oil (907.7 kg/m^3), while paraffin oil (880 kg/m^3) is lighter than rapeseed oil. The numerical results were compared to the open-eye areas recorded from the physical model.

The effect of the top layer thickness on the open-eye area

In this work, the effect of the top layer thickness on the open-eye formation was studied. For both single and dual plug systems, six cases were simulated by varying the top layer thickness while the gas flow rate was kept constant. Rapeseed oil was chosen for simulating the slag phase. The total gas flow rate in both systems was 7.5 NL/min but in dual plug system the gas flow was divided evenly for two plugs. The simulated cases are presented in Table 7. The open-eye in the physical model and in the corresponding CFD simulation is shown Figures 18–20 for Cases S6, S8 and S11, respectively. According to Figures 18–20, it is obvious that the open-eye area decreases when the top layer thickness is increased. The open-eye formation was not observed to occur when top layer thickness was increased above 7.5 cm.

Table 7. The simulated cases for studying the effect of top layer thickness on the open-eye area (Reprinted by permission from Paper IV © 2019 Wiley-VCH Verlag GmbH & Co. KGaA).

Single plug system, flow rate 7.5 NL/min						
	Case S6	Case S7	Case S8	Case S9	Case S10	Case S11
Top layer thickness [cm]	0.75	1.5	3.0	4.5	6.0	7.5
Dual-plug system, flow rate 3.75 + 3.75 NL/min						
	Case D6	Case D7	Case D8	Case D9	Case D10	Case D11
Top layer thickness [cm]	0.75	1.5	3.0	4.5	6.0	7.5

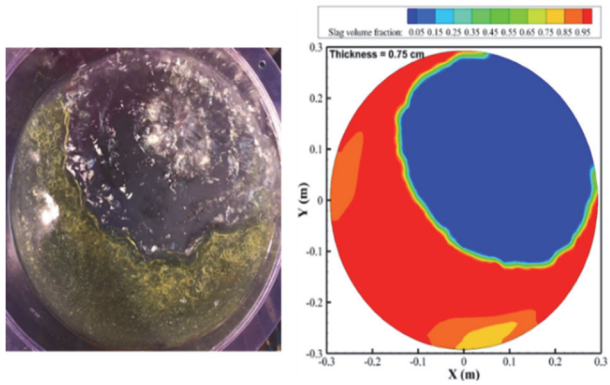

Fig. 18. The open-eye size in the physical model (left) and simulation (right) in Case S6 (Reprinted by permission from Paper IV © 2019 Wiley-VCH Verlag GmbH & Co. KGaA).

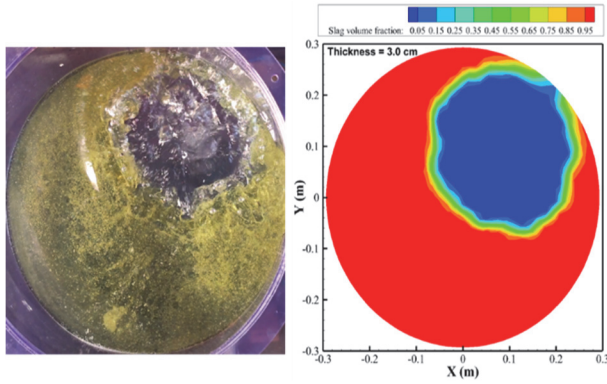

Fig. 19. The open-eye size in the physical model (left) and simulation (right) in Case S8 (Reprinted by permission from Paper IV © 2019 Wiley-VCH Verlag GmbH & Co. KGaA).

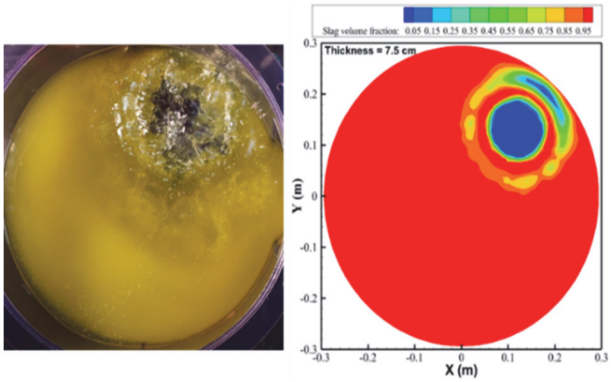

Fig. 20. The open-eye size in the physical model (left) and simulation (right) in Case S11 (Reprinted by permission from Paper IV © 2019 Wiley-VCH Verlag GmbH & Co. KGaA).

In dual plug system, two open-eyes generated merges into one single open-eye at low top layer thicknesses for a given flow rates. The increase in top layer thickness results in breaking up of single open-eye into two smaller open-eyes (Figures 21-23). As seen in Figure 21, one large open-eye was generated in case D6 that slightly starts to breaking up into two open-eyes decrease in the top layer thickness in case D8 (Figure 22). Due to further decrease in the top layer thickness, two clearly separate open-eyes are formed in case D9 (Figure 23). From these results, the top layer thickness of 4.5 cm has been identified as critical thickness which cannot to exceeded to obtain single, merged open-eye for a given gas flow rate.

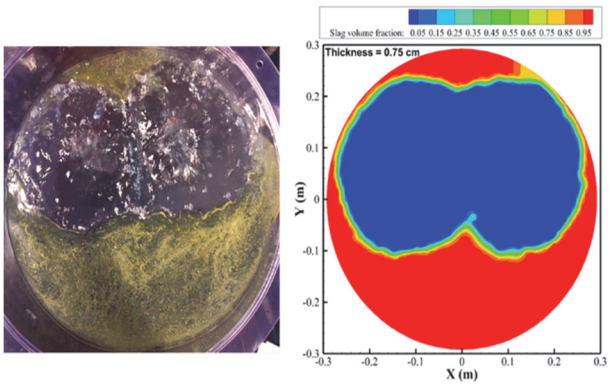

Fig. 21. The open-eye size in the physical model (left) and simulation (right) in Case D6 (Reprinted by permission from Paper IV © 2019 Wiley-VCH Verlag GmbH & Co. KGaA).

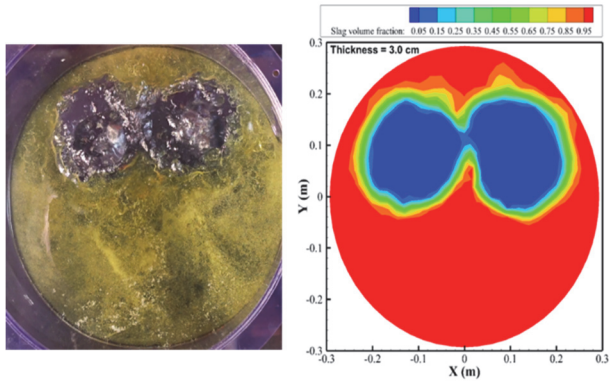

Fig. 22. The open-eye size in the physical model (left) and simulation (right) in Case D8 (Reprinted by permission from Paper IV © 2019 Wiley-VCH Verlag GmbH & Co. KGaA).

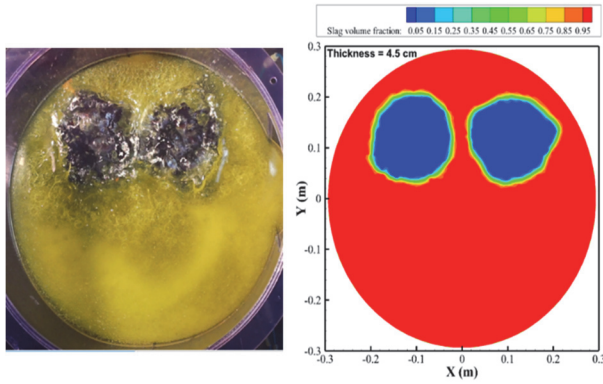

Fig. 23. The open-eye size in the physical model (left) and simulation (right) in Case D9 (Reprinted by permission from Paper IV © 2019 Wiley-VCH Verlag GmbH & Co. KGaA).

Figure. 24 a) and 24 b) present the open-eye area as a function of the top layer thickness in the single plug system and dual plug system, respectively. The quantitative results are presented in a relative form by dividing the measured open-eye area by the area of the horizontal cross-section of the ladle at the top layer height. It can be seen that the reduction of the relative open-eye area with an increase in the top layer height follows the same trend as the single plug system. In the single plug system, the mean relative error was approximately 5% while it was 12% in the dual plug system between the experimental measurements and CFD simulation results. In the dual plug system, the error is higher due to the complexity caused when two gas plumes were simulated.

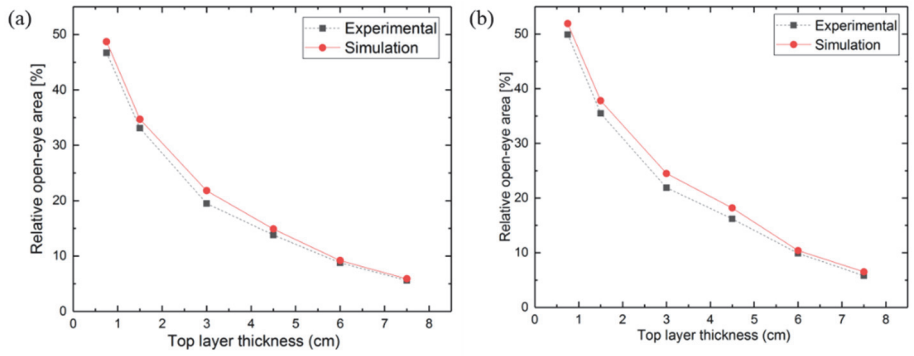

Fig. 24. The percentage of the open-eye area relative to the bath top surface area as a function of top layer thickness in a) single plug system and b) dual plug system (Reprinted by permission from Paper IV © 2019 Wiley-VCH Verlag GmbH & Co. KGaA).

As in the single plug system, the top layer thickness has a significant effect on the formation of the open-eye, when gas is injected from two plugs. From the results, it can be concluded that the top layer thickness has a significant effect on the formation of the open-eye. For industrial practice, this means that a thicker slag layer needs to be compensated for with a higher gas flow rate. It would be beneficial to use dual plug system when there is a lower top layer thickness, because it would reduce the deformation of the top layer and a larger open-eye is formed by the merging of the two slag eyes generated, which is better suited for alloying compared to a single plug system. On the other hand, it is not suggested to use a dual plug system when using a higher top layer thicknesses, because of the weakened plumes through increment of plugs tend to generate smaller open-eyes compared to single plug system, which may not be good for alloying.

Furthermore, the dimensionless open-eye area was calculated with the mechanistic model developed by Krishnapisharoday and Irons [17]. The predicted trend of the dimensionless open-eye showed good agreement when compared to the experimental data available in the literature. The experimental data collected by various authors and the meanings of the non-dimensional parameters in Figures 25 a) and 25 b) can be found in reference [17]. The parameters used in the 25 a) and 25 b) are shown in the Equation (16) and Equation (17) below.

$$\frac{A_e^*}{A_p^*} = (Q^*)^{1/3}\left(\frac{H}{h}\right)^{1/2}, \tag{16}$$

$$\frac{A_e^*}{A_p^*} = (1-\rho^*)^{-1/2}(Q^*)^{1/3}(\frac{H}{h})^{1/2}. \quad (17)$$

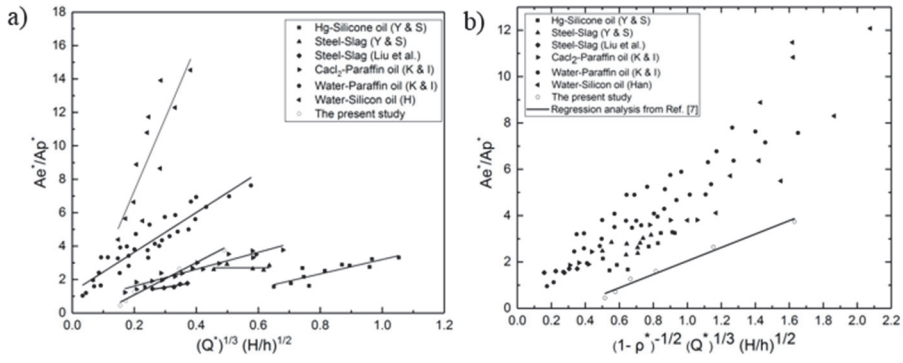

Fig. 25. Variation of non-dimensional open-eye ratio compared to the literature (K&I: Krishnapisharody and Irons [17]; Yonezawa and Schwerdtfeger [14]; H. Han et al. [72]: (Reprinted by permission from Paper IV © 2019 Wiley-VCH Verlag GmbH & Co. KGaA).

The effect of the top layer density on the formation in single and dual-plug configurations

To investigate the effect of top layer densities on the open-eye area, experiments were conducted using two additional oils. The oils were chosen based on their density: castor oil (956 kg/m^3) is heavier than rapeseed oil (907.7 kg/m^3), while paraffin oil (880 kg/m^3) is lighter. The top layer thickness of 3.0 was used in all the experiments and results were compared with the measurements conducted using rapeseed oil. The images of the formed open-eye from the experiments and simulations in the single-plug system can be seen in Figure 26 and for dual-plug system in Figure 27.

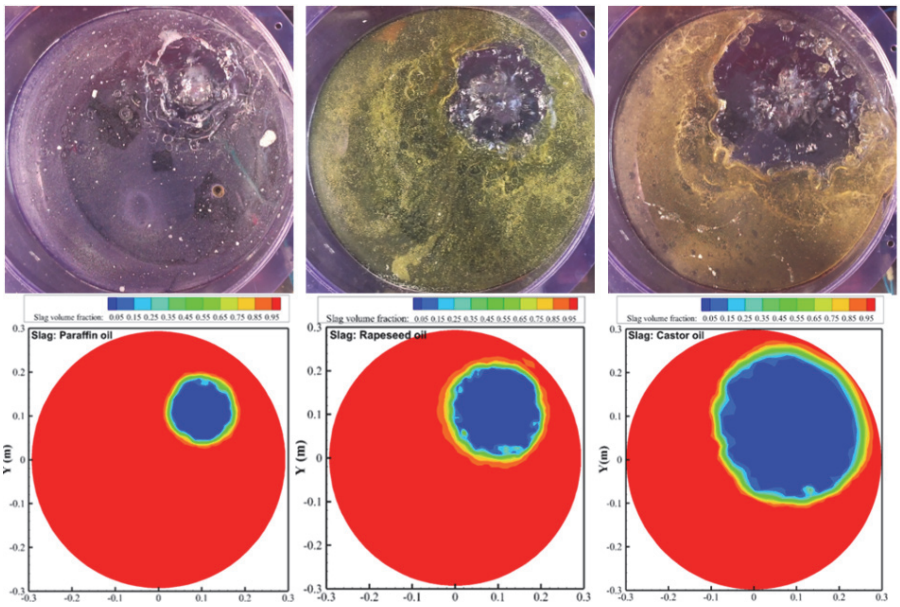

Fig. 26. The physical model (top) and simulation (bottom) results for the open-eye size in a single plug system for different top layer properties: paraffin oil (on the left), rapeseed oil (in the middle) and castor oil (on the right) (Reprinted by permission from Paper IV © 2019 Wiley-VCH Verlag GmbH & Co. KGaA).

As seen from the Figure 26, the open-eye size enlarges with an increase in the density of the top layer. The largest open-eye was formed using the densest oil (castor oil) and smallest open-eye was formed using low-density oil (paraffin oil). Similar results for dual-plug system are presented in Figure 27. For the castor oil (densest), one merged open-eye is formed and with the rapeseed and paraffin oils (low-density) two separate open-eye are formed. The results suggest that a larger open-eye is formed when slag density is higher for an injected flow rate, which might suit for better alloying purpose.

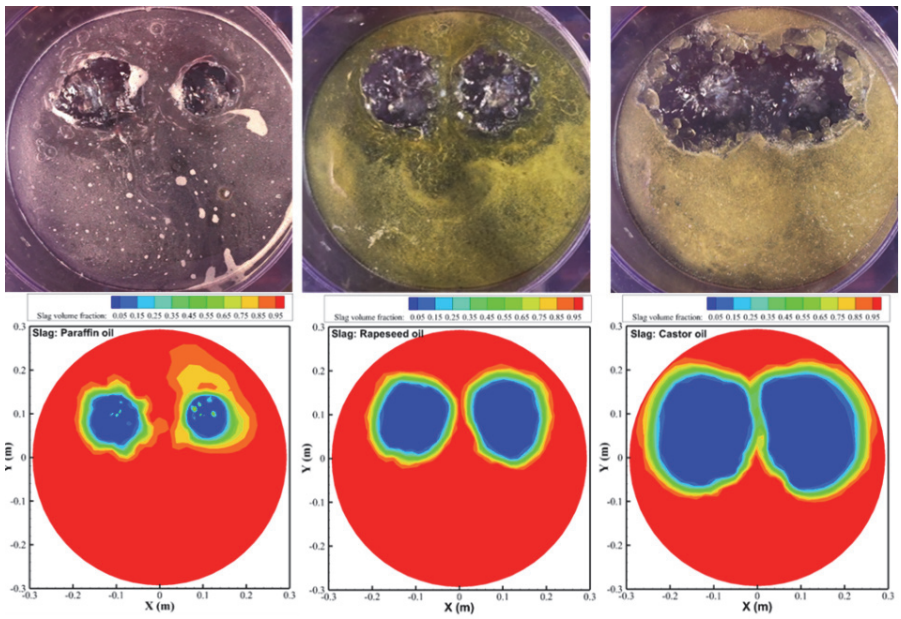

Fig. 27. The physical model (top) and simulation (bottom) results of the open-eye size in a dual-plug system for different top layer properties: paraffin oil (on the left), rapeseed oil (in the middle) and castor oil (on the right) (Reprinted by permission from Paper IV © 2019 Wiley-VCH Verlag GmbH & Co. KGaA).

The predicted behaviour of the open-eye sizes with respect to the top layer properties was consistent with the experimental results of Krishnapisharody and Irons [16] and Wu, Valentin and Sichen [18]. Krishnapisharody and Irons [6] also performed similar measurements studying the effect of the top layer density and viscosity using less dense paraffin oil and denser motor oil on the open-eye size. Krishnapisharody and Irons [16] concluded that the change in the open-eye was attributed mainly to the differences in the density of the top layer, while the dynamic viscosity of the top layer player plays virtually no role. Wu, Valentin and Sichen [18] also carried out measurements studying the open-eye size using water model experiments. Their results indicated that the gas flow rate as well as the height of the lower and top liquids have a strong impact on the open-eye size, while the viscosity of the top layer and the interfacial tension have only a little effect on the open-eye size.

4.3 Open-eye formation in an industrial scale ladle for different operating parameters

In Paper V, the effect of the gas flow rate and slag layer thickness on the open-eye formation in an industrial scale ladle was studied. The ladle studied in this work was a 150-ton ladle at the Outokumpu Stainless Oy, Tornio plant in Finland. The simulations were performed with gas flow rates varying from 200 to 500 NL/min and a slag layer thickness varying from 25 to 55 cm. The numerical simulations of the open-eye area were compared to the industrial measurements.

Table 8. The simulated cases for studying the effect of the gas flow rate and slag layer thickness on the open-eye formation.

Slag layer thickness (cm)	40 (base case)	55	25
Gas flow rate (NL/min)		Cases	
200	R1	R4	R7
400	R2	R5	R8
500	R3	R6	R9

4.3.1 The effect of the gas flow rate on the open-eye formation

Figures 28 and 29 show the argon gas propagation and the open-eye formation process at the beginning of gas stirring for flow rates of 200 and 500 NL/min (Case R1 and R3). The argon gas was injected into the steel bath through a nozzle breaks up into gas bubbles and infringe the slag layer at high flow rates forming an open-eye. In the case R3, when the argon gas flow rate is 500 NL/min, the time taken for the argon gas to reach the slag layer appears to be shorter (see Figure 29) when compared to R1 operated with flow rate of 200 NL/min (Figure 28). The open-eye formation has already been observed in case R3 at a physical time of 3.0 seconds (see Figure 29 b)), while in the case R1, it is completely formed (see Figure 28 b)).

a) At time = 1.5 sec b) At time = 3.0 sec c) At time = 4.5 sec

Fig. 28. The argon floating and open-eye formation process for a flow rate of 200 NL/min (Case R1) (Reprinted by permission from Paper V © 2019 Authors).

a) At time = 1.5 sec b) At time = 3.0 sec c) At time = 4.5 sec

Fig. 29. The argon floating and open-eye formation process for a flow rate of 500 NL/min. (Case R3) (Reprinted by permission from Paper V © 2019 Authors).

Figure 30 shows the experimental and simulation results of the effect of the argon flow rate on the open-eye area for a slag layer thickness of 40 cm. Due to the dynamic nature of the open-eye size and position, the open-eye area was averaged over a period of 60 seconds. Even an argon flow rate of 200 NL/min (R1) was able

to break the slag layer and generate a smaller open eye in experiments and in the simulations. The open-eye formation did not appear when the industrial scale ladle operated with an argon flow rate of less than 200 NL/min.

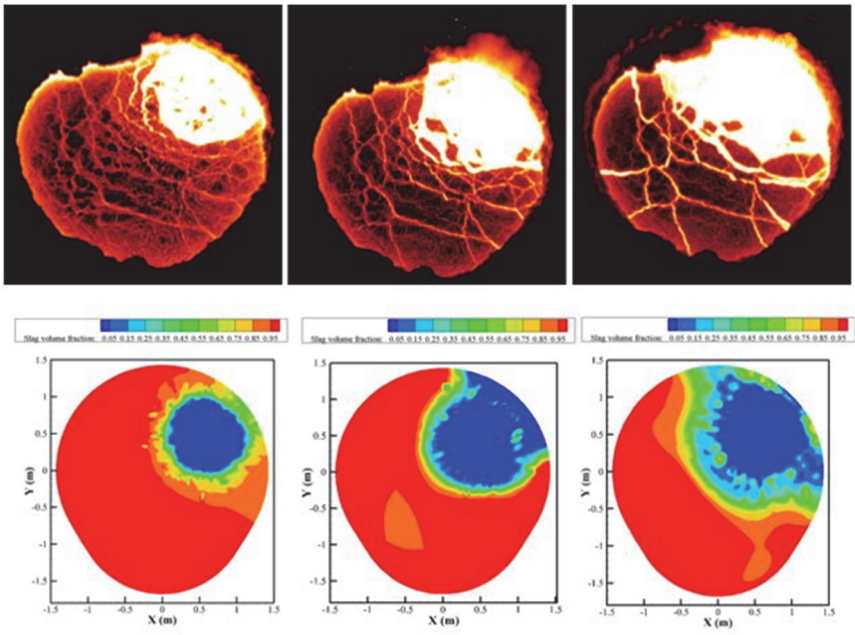

Fig. 30. The experimental (top) and simulation (bottom) results of open-eye area for a slag layer thickness of 40 cm and different gas flow rates: R1 (left), R2 (in the middle) and R3 (on the right) (Reprinted by permission from Paper V © 2019 Authors).

The position of the open-eye tends to move closer to the ladle wall at high flow rates (cases R2 and R3) resulting in the increase of the fluid flow velocities near to the ladle wall. In industrial practice, this would contribute to the high refractory wear and thus reduce the ladle life. Valentin et al. [42] also predicted the same trend of increase open-eye area with increase in the argon flow rates. The simulation results open-eye area were in good agreement when compared to the simulation results of Liu, Qi and Xu [43] and Li, Yin and Zhu [44].

The dynamic behaviour of the open-eye area with time for experimental and simulation results for cases R1, R2 and R3 is shown in the Figure 31. Depending on the flow rates operated, the open-eye area expands rapidly and reaches a peak value. However, the time taken to reach the peak does not depend on the flow rate

and it is same in all the cases R1, R2 and R3. The open-eye starts to decrease after reaching the peak value and starts to fluctuate around a constant level once it is stabilised. For flow rates of 200, 400 and 500 NL/min, the peak values of open-eye area are 1.6 m^2, 3.2 m^2 and 5.0 m^2 and time-averaged values are 0.7 m^2, 1.59 m^2 2.3 m^2 respectively in the simulation results.

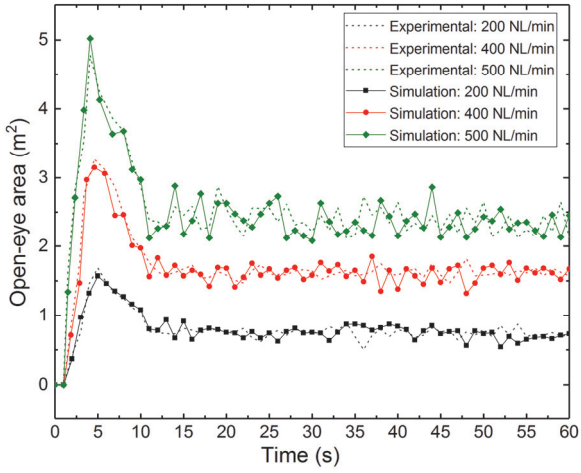

Fig. 31. The variation of the area over time for both experiments and simulations (Reprinted by permission from Paper V © 2019 Authors).

The experimental and simulation results of the influence of increase in slag layer thickness to 55 cm from 40 cm on open-eye area with different flow rates is shown in Figure 32. The lowest argon flow rate of 200 NL/min (R4) was not sufficient to break the slag layer and formation of open-eye was not possible with the increment of slag layer thickness (see Figure 32 (left)). The open-eye formation follows the same trend, but with a reduction in the open-size to some extent in the cases R5 and R6.

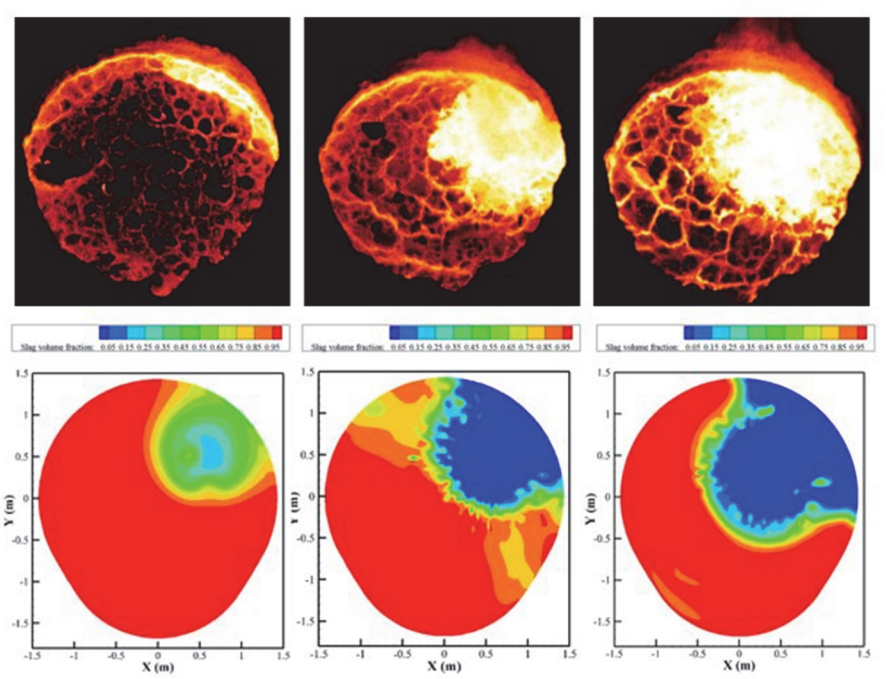

Fig. 32. The experimental (top) and simulation (bottom) results of the open-eye area for a slag layer thickness of 55 cm for cases R4 (left), R5 (in the middle) and R6 (on the right) (Reprinted by permission from Paper V © 2019 Authors).

The experimental and simulation results of the open-eye formation when the slag layer thickness was reduced to 25 cm, cases R7, R8 and R9 are shown in Figure 33. The open-eye formation in the cases R7 and R8 follows the same trend as in the cases R1 and R2 but with an increase in the open-eye size and more dynamic behaviour. At a higher argon flow rate in the case R9 (500 NL/min), the open-eye formation follows the same trend as R3, but the open-eye size is very large. Moreover, there is huge deformation of slag layer and size of the open-eye is almost half of the ladle cross-sectional area.

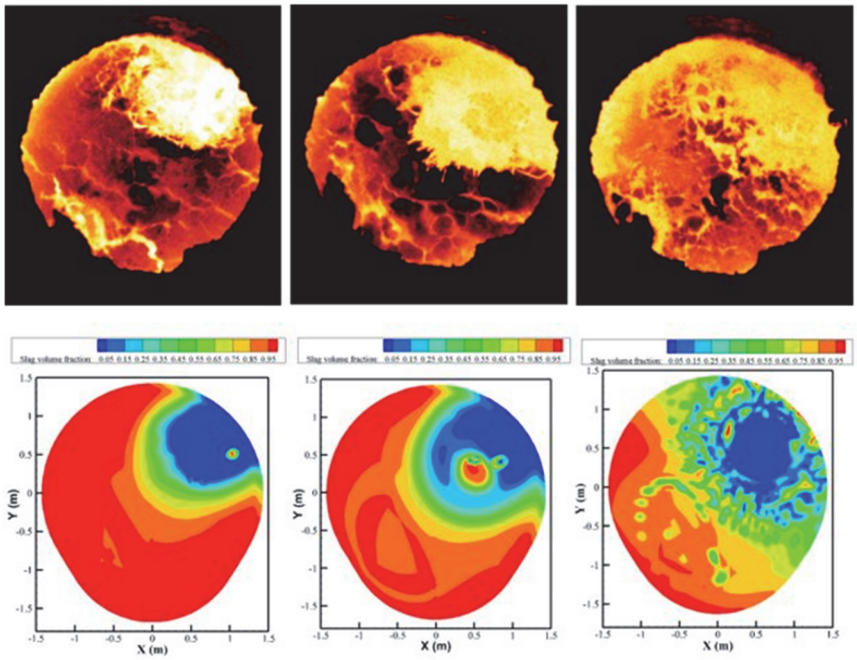

Fig. 33. The experimental (top) and simulation (bottom) results of open-eye area for a slag layer thickness of 25 cm for cases R7(left), R8 (in the middle) and R9 (on the right) (Reprinted by permission from Paper V © 2019 Authors).

4.3.2 Comparison of open-eye area with different gas flow rates and slag layer thickness

Table 9 presents the summary of all the experimental and simulation results of the open-eye areas when the gas flow rate is increased from 200 to 500 NL/min and the slag layer height increased from 25 to 55 cm, i.e. for cases R1 to R9.

Table 9. Summary of experimental and simulated values from cases R1 to R9 (Reprinted by permission from Paper V © 2019).

Slag layer thickness (cm)	40 (base case)			55			25		
Gas flow rate (NL/min)	Case	Exp (m^2)	Sim (m^2)	Case	Exp (m^2)	Sim (m^2)	Case	Exp (m^2)	Sim (m^2)
200	R1	0.7	0.69	R4	NA	NA	R7	1.08	0.95
400	R2	1.58	1.59	R5	1.32	1.44	R8	1.82	1.89
500	R3	2.24	2.30	R6	1.81	1.95	R9	NA	NA

Overall, the same trend in followed in experiments and simulations with increase in open-eye area with increase in flow rate and reduction in open-eye area with increment in slag layer thickness. In case R4, when the slag layer height is increased to 55 cm, the flow rate of 200 NL/min was not sufficient enough to break the slag layer and generate open-eye. On the other hand, the open-eye generated was more dynamic in the case R9, when slag layer height of 25 cm and flow rate of 500 NL/min was used.

The comparison between the experimental and simulation values of the open-eye area for different slag layer thicknesses is displayed in Figure 34. The simulation results are in good agreement with the experimental ones. The results indicate that the gas flow rate and slag layer height play a pivotal role in generating a suitable open-eye size for alloying purposes. A thick slag layer needs to be compensated for a higher gas flow rate in order to keep open-eye constant.

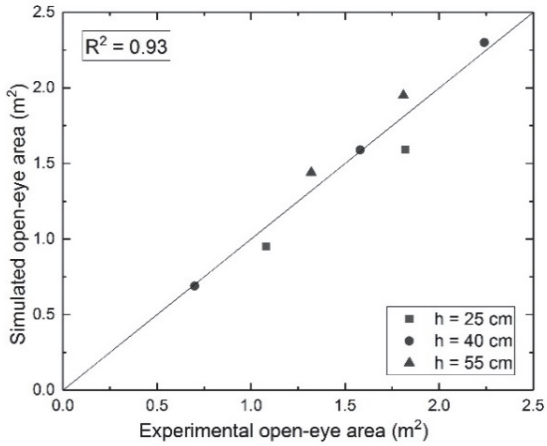

Fig. 34. A comparison between experimental and simulated values of open-eye areas (Reprinted by permission from Paper V © 2019 Authors).

4.4 Mixing time distribution in industrial scale ladle

In the Paper VI, the effect of gas flow rate on the mixing phenomena on an industrial scale was studied. The industrial measurements of the mixing time were performed at Outokumpu Stainless Oy in Tornio, Finland. During the experiments, steel samples of concentration were taken from the ladle at certain intervals of time and at a certain location. The nickel alloying to the steel was done at sampling point 0 to reach a case-specific nickel content. Steel samples were then used to evaluate the required mixing time to obtain the desired nickel content starting from point of alloying. The simulations were performed using the same computational domain as used in Paper V. A slag layer thickness of 35 cm was used, and the simulations were performed with gas flow rates of 100, 300 and 500 NL/min. The simulation results of the mixing time were compared to the industrial measurements available from Outokumpu.

Figure 34 displays the locations of the points inside the ladle where mixing time is calculated. In simulations, a tracer in the form of a circle with a radius of 0.196 m was released to simulate the nickel alloy at a point where the gas bubble plume breaks the slag layer and creates the open-eye. The mixing time in this study was defined as the time needed to reach a 95% degree of homogenization in the molten steel. In the simulations, shell formation and melting of the alloy was ignored.

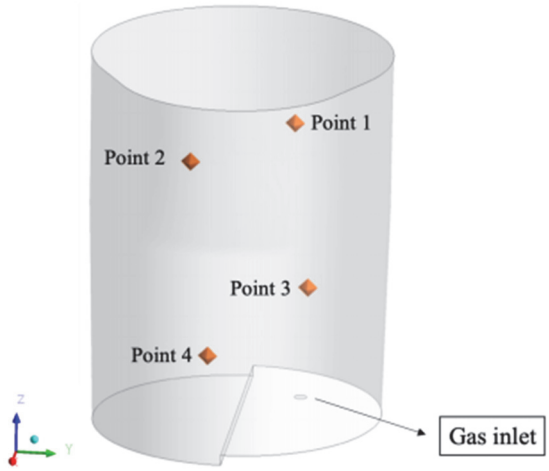

Fig. 35. Monitoring points for the calculating the mixing time inside the ladle (Reprinted by permission from Paper VI © 2019 Authors).

The concentration profiles of the tracer inside the ladle for different flow rates after the addition times of 0 s, 5 s, 10 s, 20 s, 40 s and 60 s is shown in Figure 36. The tracer is injected into the molten steel at time 0 s at the point above the open-eye (see Figure 36 a)). Figure 36 b) depicts the dissolution of the tracer into the molten steel at 5 s and also the tracer movement, which is moving to the other direction due to the high gas flow coming through the nozzle. At high flow rate of 500 NL/min, the dissolution of the tracer is higher when compared to low gas flow rate of 200 NL/min. As seen in Figure 36 c) and Figure 36 d), the same trend was followed. For gas flow rate of 500 NL/min, the tracer has spread out almost throughout the whole ladle at 40 s (see Figure 36 e)), while it is 65% dissolved for flow rate of 100 NL/min. At 60 s, the tracer was completely spread out when the ladle furnace was operated at high flow rate of 500 NL/min and almost spread out for other gas flow rates (see Figure 36 f)).

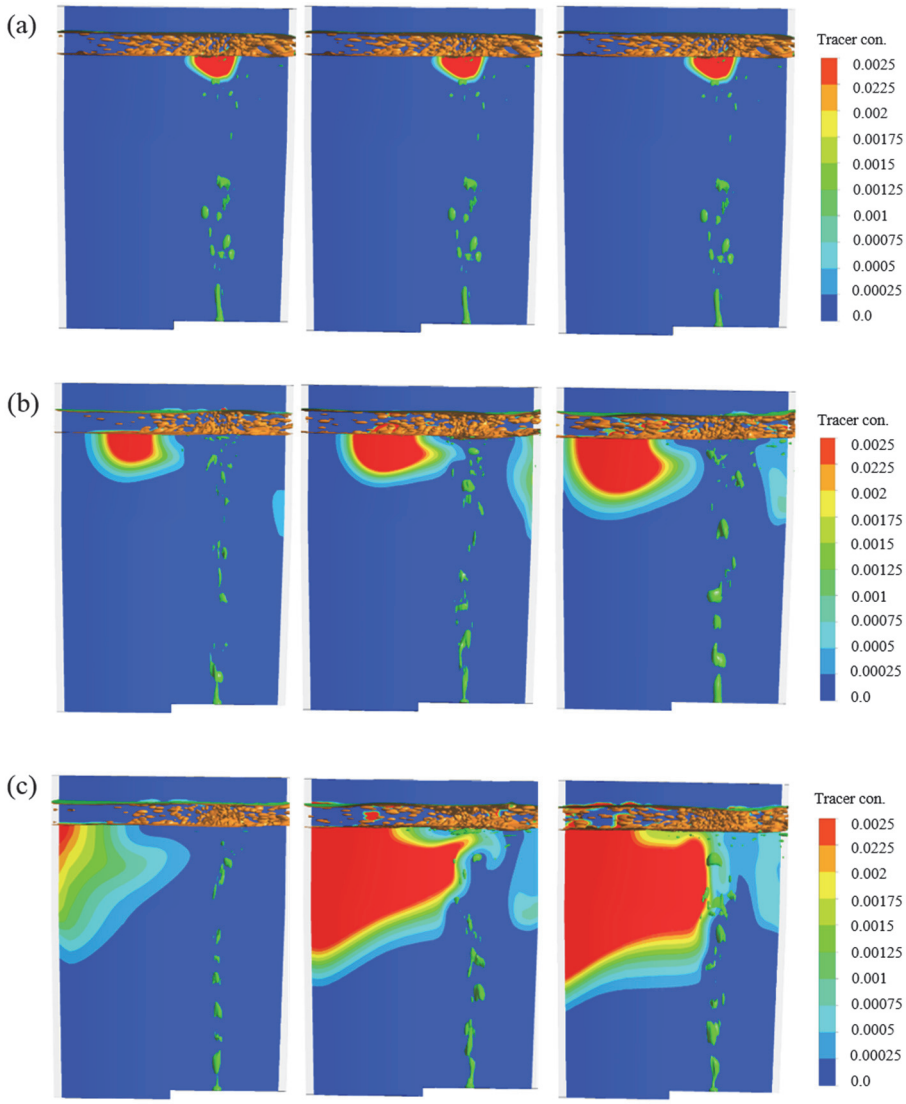
(a)
Tracer con.
0.0025
0.0225
0.002
0.00175
0.0015
0.00125
0.001
0.00075
0.0005
0.00025
0.0
(b)
Tracer con.
0.0025
0.0225
0.002
0.00175
0.0015
0.00125
0.001
0.00075
0.0005
0.00025
0.0
(c)
Tracer con.
0.0025
0.0225
0.002
0.00175
0.0015
0.00125
0.001
0.00075
0.0005
0.00025
0.0

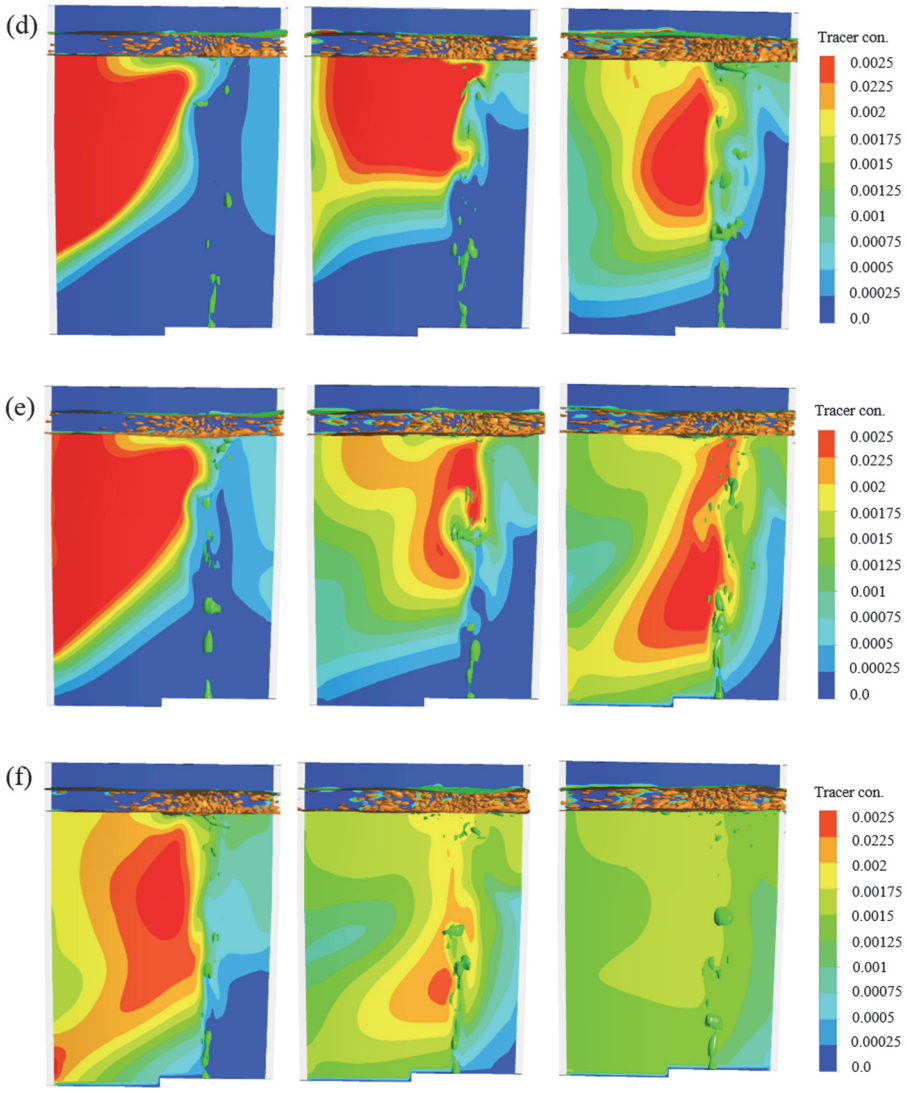

Fig. 36. Tracer concentration profiles for gas flow rates of 100 NL/min (left), 300 NL/min (middle) and 500 NL/min (right) at different time intervals: (a) 0 s (b) 5 s (c) 10 s (d) 20 s (e) 40 s, and (f) 60 s (Reprinted by permission from Paper VI © 2019 Authors).

The procedure adopted to calculate the 95% mixing time for various gas flow rates and typical tracer response curves of four monitoring points are showed in Figures 37 a), 37 b) and 37 c). Figure 37 d) depicts the average mixing time value at Point

1 from the numerical simulations and industrial measurements. At a certain location, steel samples of the concentration were taken from the ladle during the experiments at different intervals of time. To evaluate the mixing time for obtaining an aimed nickel content, steel samples were then used starting from the point of alloying.

The results indicate that mixing time decreases with increase in the gas flow rate in the experiments and simulations. The present results are in good agreement when compared to the industrial scale simulation results of Liu et al. [25]. The maximum error between the industrial measurements and simulation results is of 16.3% and possible source for that is the tracer addition method and ignoring of subsequent melting of alloy in the simulations.

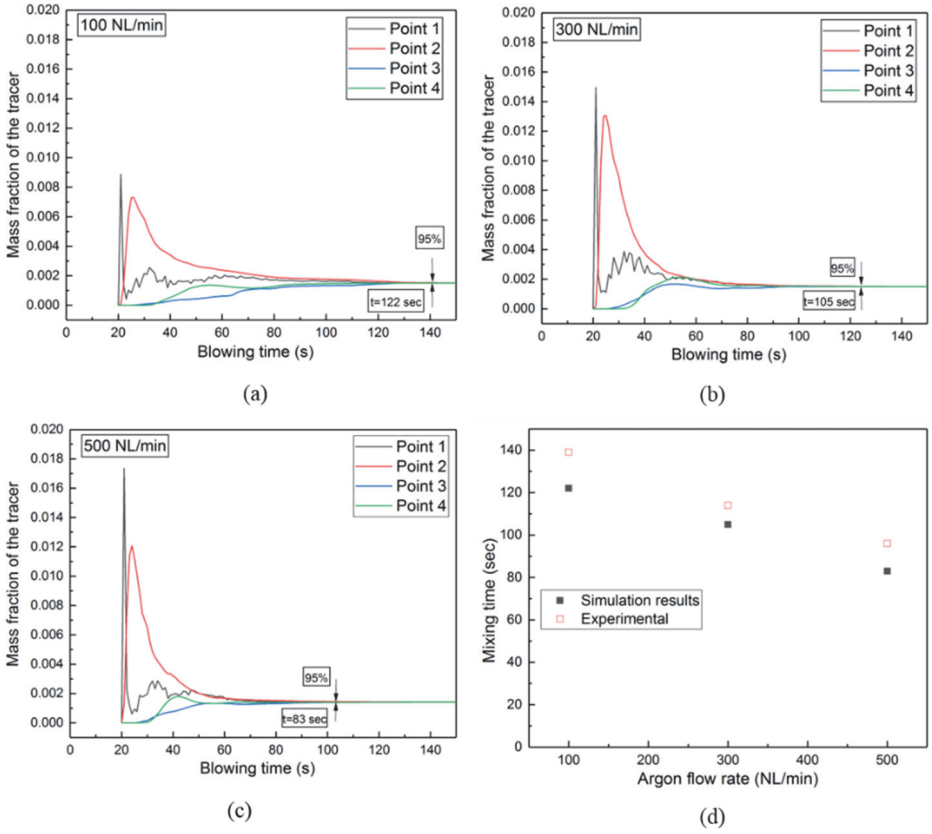

Fig. 37. Tracer concentration change for different gas flow rates (a) 100 NL/min (b) 300 NL/min (c) 500 NL/min. (d) A comparison of the simulated average mixing time for

different gas flow rates with experimental values (Reprinted by permission from Paper VI © 2019 Authors).

5 Conclusions and future work

In this work, the effect of different operating parameters on the open-eye formation process and mixing behaviour in a gas-stirred ladle was studied. A CFD model was developed using a multi-phase Volume of Fluid (VOF) model. The simulation results were validated against data obtained from physical modelling and industrial measurements.

In Paper I, simulations were carried out to validate the experimental data available in the literature. A detailed comparison was made for simulation results of the liquid flow velocities at different heights in the ladle with experimental measurements. A 1:5 scale water model of a 150-ton industrial ladle was used for physical modelling to obtain validation data for the CFD model. In the physical model, water and air were used to represent liquid steel and argon, respectively. The effect of the gas flow rate, number of nozzles, top layer (oil/slag) thickness and density on the open-eye size were studied. It was found that the open-eye size increased with an increase in the gas flow rate for both single and dual-plug configurations. At a given flow rate, the flow velocity in the vicinity of the ladle wall tended to decrease in the dual-plug system when compared to the single plug system. The increase in the number of porous plugs results in a larger open-eye and could also reduce the wear of the ladle refractory. The open-eye area was found to decrease with an increase in the top layer thickness in single and dual-plug configurations. To study the effect of top layer densities on the open-eye area, experiments and simulations were conducted using castor oil (heavier than rapeseed oil) and paraffin oil (lighter than rapeseed oil). The results showed that, the top layer with a high density (castor oil) generated a larger open-eye when compared to the top layer with a lower density (paraffin oil). Under the conditions of the work, the dynamic viscosity of the top layer did not have a significant effect on the open-eye area.

After validation with the water model, the developed CFD approach was extended to simulate a 150-ton industrial ladle. To validate the model, the open-eye formation in an industrial ladle was captured using an IR camera. It was concluded that the argon flow rate and slag layer thickness have a significant effect on the open-eye size in the ladle. The open-eye increases from 10.3 to 33.1% of the ladle's free top surface area with an increase in the flow rate from 200 to 500 NL/min and with a 40 cm slag layer thickness. The reduction of the slag layer thickness from 40 to 25 cm resulted in a much larger deformation of the slag layer and more a rapidly fluctuating open-eye at a high flow rate of 500 NL/min. When the slag layer

thickness was increased from 40 to 55 cm, the gas flow rate of 200 NL/min was not strong enough to break the slag layer and formation of open-eye was not possible.

Finally, a species transport model was used to calculate the mixing time in the ladle. The results suggest that the mixing time decreases with increases in the gas flow rate. The simulation results for the mixing time agree fairly well with the industrial measurements, with a maximum error of 16.3%. A possible source of the error between the experiments and the simulations is the tracer addition method and due to ignoring the shell formation and subsequent melting of the alloy in the simulations.

As for future work, the development of the model could continue by combining the Large Eddy Simulation (LES) approach coupled with Discrete Particle Modelling (DPM) to study the slag droplets and bubble movements in the ladle. Another possible task would be to develop the model to simulate the shell formation procedure for alloying elements in the ladle.

List of references

1. J. Szekely, H. J. Wang and K. M, “Flow pattern velocity and turbulence energy measurements and predictions in a water model of an argon stirred ladle”, *Metall. Mater. Trans. B,* vol. 7, pp. 287–295, June. 1975.
2. O. J. Ilegbusi, J. Szekely, M. Iguchi, H. Takeuchi and Z.-I. Morita, “A Comparison of Experimentally Measured and Theoretically Calculated Velocity Fields in a Water Model of an Argon Stirred Ladle,” *ISIJ Int*., Vol. 33, pp. 474–478, Jan. 1993.
3. Y. Xie and F. Oeters, “Experimental studies on the flow velocity of molten steels in a ladle at centric gas blowing”, *Steel Res*., vol. 63, pp. 93–104, March. 1992.
4. Y. Xie, S. Orsten and F. Oeters, “Behaviour of Bubbles at Gas Blowing into Liquid Wood’s meta”, *ISIJ Int*., vol. 32, pp. 66-75, Sep. 1991.
5. J. L. Xia, T. Ahokainen and L. Holappa, “Modelling of Flows in a Ladle with Gas Stirred Liquid Wood’s Metal”, Proceedings of the Second International Conference on CFD in the *Minerals and Process Industries, CSIRO*, Melbourne, Australia, December 6-8, 1999, pp. 187-192.
6. W. Lou and M. Miaoyong Zhu, “Numerical Simulation of Gas and Liquid Two-Phase Flow in Gas-Stirred Systems Based on the Euler–Euler Approach”, *Metall. Mater. Trans. B*, vol. 44, pp.1251-1263, Oct. 2013.
7. C. G. Mendez, N. Nigro and A. Cardona, “Drag and non-drag influences in numerical simulations of metallurgical ladles”, *J. Mater. Process. Technol*., vol 160, pp. 296–305, June. 2014.
8. H. Türkoğlu and B. Farouk, “Numerical computations of fluid flow and heat transfer in a gas-stirred liquid bath”, *Metall. Mater. Trans. B,* vol. 21 pp. 771–781, June. 1990.
9. M. R. Davidson, “Numerical calculations of two-phase flow in a liquid bath with bottom gas-injection: The central plume”, *Appl. Math. Model*., vol. 14, pp. 67–76, Feb. 1999.
10. J. F. Domgin, P. Gardin and M. Brunet, “Experimental and numerical investigations of gas stirred ladles”, Proceedings of the *Second International Conference on CFD in the Minerals and Process Industries*, Melbourne, Australia, CSIRO, Melbourne, Australia, December 6-8, 1999, pp. 181-186.
11. H-J. Park and W-J. Yang, “Turbulent two-phase mixing in gas-stirred systems for continuous casting applications”, *Numer. Heat Tr. A-Appl.,* vol. 31, pp. 493–515, March. 1997.
12. Y. Liu, M. Ersson, H. Liu, P. G. Jönsson and Y. Gan, “A Review of Physical and Numerical Approaches for the Study of Gas Stirring in Ladle Metallurgy”, *Metall. Mater. Trans. B,* vol. 50, pp. 555–577, Feb. 2019.
13. K. Yonezawa and K. Schwerdtfeger, “Spout Eyes Formed by an Emerging Gas Plume at the Surface of a Slag-Covered Metal Melt”, *Metall. Mater. Trans. B,* vol. 30, pp. 411–418, June. 1999.
14. K. Yonezawa and K. Schwerdtfeger, “Height of the Spout of a Gas Plume Discharging from a Metal Melt”, *Metall. Mater. Trans. B*, vol. 30, pp. 655-660, Aug. 1999.

15. K. Yonezawa and K. Schwerdtfeger, “Dynamics of the Spout of Gas Plumes Discharging from a Melt: Experimental Investigation with a Large-Scale Water Model”, *Metall. Mater. Trans. B*, vol. 31, pp. 461-468, June. 1999.
16. K. Krishnapisharodoy and G. A. Irons, “Modeling of Slag Eye Formation over a Metal Bath Due to Gas Bubbling”, *Metall. Mater. Trans. B,* vol. 37, pp.763–772, Oct. 2006.
17. K. Krishnapisharodoy K and G.A. Irons, “An Extended Model for Slag Eye Size in Ladle Metallurgy”, *ISIJ Int*., vol. 48, pp. 1807–1809, Aug. 2008.
18. L. Wu, P. Valentin and D. Sichen, “Study of Open Eye Formation in an Argon Stirred Ladle”, *Steel Res Int*., vol. 8, pp. 508–515, April. 2010.
19. M. Thunman, S. Eckert, O. Hennig, J. Bkörkvall and Du. Sichen, “Study on the Formation of Open-eye and Slag Entrainment in Gas Stirred Ladle”, *Steel Res Int*., vol. 78, pp. 849–856, June. 2007.
20. A. M. Amaro-Villeda, M. A. Ramirez-Argaez and A. N. Conejo, “Effect of Slag Properties on Mixing Phenomena in Gas Stirred Ladles by Physical Modelling”, *ISIJ Int*., vol. 54, pp. 1–8, Aug. 2014.
21. A. Maruyama and M. Iguchi, “Cold Model Study of Spout Eye Area in the Presence of the Slag Layer Simulated by Low-Density Particles”, *J. JSEM*, vol. 12, pp. 7-10, April. 2012.
22. D. Mazumdar, P. Dhandpani and R. Saravanakumar, “Modelling and Optimization of Gas Stirred Ladle Systems”, *ISIJ Int*., vol. 57, pp. 286–295, Oct. 2017.
23. Z. Liu, L. Li and B. Li, “Modeling of the Gas-Steel-Slag Three-Phase Flow in Ladle Metallurgy: Part 1. Physical Modeling”, *ISIJ Int*., vol. 57, pp.1971-1979, June. 2017.
24. L. Li, Z. Liu, B. Li, H. Matsuura and T. Fumitaka, “Water Model and CFD-PBM Coupled Model of Gas-Liquid-Slag Three-Phase Flow in Ladle Metallurgy”, *ISIJ Int*., vol.55, pp. 1337-1346, Feb. 2015.
25. L. Li, Z. Liu, M. Cao and B. Li, “Large Eddy Simulation of Bubble Flow and Slag Layer Behaviour in Ladle with Discrete Phase Model (DPM)-Volume of Fluid (VOF) Coupled Model”, *JOM*, vol. 67, pp. 1459-1467, June. 2015.
26. L. Li and B. Li, “Investigation of Bubble-Slag Layer Behaviours with Hybrid Eulerian-Lagrangian Modeling and Large Eddy Simulation”, *JOM*, vol. 68, pp. 2160-2169, March. 2016.
27. F. A. Calderon-Hurtado, R. M. Davila, K. Chattopadhyay and S. Garcia-Hernandez, “Fluid Flow Turbulence in the Proximities of the Metal-Slag Interface in Ladle Stirring Operations”, *Metals*, vol. 9, pp. 1-17, Feb. 2019.
28. W. Liu, H. Tang, S. Yang, M. Wang, J. Li, Q. Liu and J. Liu, “Numerical Simulation of Slag Eye Formation and Slag Entrapment in a Bottom-Blown Argon-Stirred Ladle”, *Metall. Mater. Trans. B*, vol. 49, pp. 2681-2691, Oct. 2018.
29. L. Li, B. Li and Z. Liu, “Modeling of Gas-Steel-Slag Three-Phase Flow in Ladle Metallurgy: Part II. Multi-scale Mathematical Model”, *ISIJ Int*., vol. 57, pp.1980–1989, Oct. 2017.
30. N.-N. Lv, L.-S. Wu, H.-C. Wang, Y.-Y. Dong and C. Su, “Size Analysis of Slag Eye Formed by Gas Blowing in Ladle Refining”, *J. Iron Steel Res. Int*., vol. 24, pp. 243-250, March. 2017.

31. D. Mazumdar and R. I. L. Guthrie, “On Mathematical Models and Numerical Solutions of Gas Stirred Ladle Systems”, *Appl. Math. Model*., vol. 17, pp. 255-262, May. 1993.
32. D. Mazumdar D and R. I. L. Guthrie, “Numerical Computation of Flow and Mixing in Ladle Metallurgy Steelmaking Operations (C.A.S method)”, *Appl. Math. Model*., vol. 10, pp. 25-32, Feb. 1986.
33. D. Mazumdar D and R. I. L. Guthrie, “The Physical and Mathematical Modelling of Gas Stirred Ladle Systems”, *ISIJ Int*., vol. 35, pp.1–20, Sep. 1995.
34. D. Mazumdar, R. Yadhav and B. Mahato, “Transient Flow and Mixing in Steelmaking Ladles during the Initial Period of Gas Stirring”, *ISIJ Int*., vol. 42, pp.106–108, Sep. 2002.
35. D. Mazumdar and J. W. Evans, “A Model for Estimating Exposed Plume Eye Area in Steel Refining Ladles Covered with Thin Slag”, *Metall. Mater. Trans. B*, vol. 35, pp. 400-404, April. 2004.
36. J. Mandal, S. Patil, M. Madan and D. Mazumdar, “Mixing Time and Correlation for Ladles Stirred with Dual Plugs”, *Metall. Mater. Trans. B*, vol. 36, pp. 479-487, Aug. 2005.
37. M. Peranadhanthan and D. Mazumdhar, “Modeling of Slag Eye in Argon Stirred Ladles”, *ISIJ Int*., vol. 50, pp. 1622-1631, Aug. 2010.
38. M. Madan, D. Satish and D. Mazumdar, “Modeling of Mixing in Ladles Fitted with Dual Plugs”, *ISIJ Int*., vol. 45, pp. 677-685, Feb. 2005.
39. S. P. Patil, D. Satish, M. Peranandhanathan and D. Mazumdar, “Mixing Models for Slag Covered, Argon Stirred Ladles”, *ISIJ Int*., vol. 50, pp.1117-1124, June. 2010.
40. Subagyo, G. A. Brooks and G. A. Irons, “Spout Eyes Area Correlation in Ladle Metallurgy”, *ISIJ Int*., vol 43, pp. 262-263, Oct. 2003.
41. D. C. Guo, L. Gu and G. A. Irons, “Developments in Modelling of Gas Injection and Slag Foaming”, *Appl. Math. Model*., vol. 26, pp. 263-280, April. 2002.
42. P. Valentin, C. Bruch, Y. Kyrylenko, H. Köchner and C. Dannert, “Influence of the Stirring Gas in a 170-t Ladle on Mixing Phenomena-Formation and On-line Control of Open-Eye at an Industrial LD Steel Plant”, *Steel Res Int*., vol. 80, pp. 552–558, March. 2009.
43. H. Liu, Z. Qi and M. Xu, “Numerical Simulation of Fluid Flow and Interfacial Behaviour in Three-phase Argon-Stirred Ladles with One Plug and Dual Plugs”, *Steel Res Int*., vol. 82, pp. 440–458, Nov. 2011.
44. B. Li, H. Yin, C. Q. Zhou and F. Tsukihashi, “Modeling of Three-phase Flows and Behaviour of Slag/Steel/Interface in an Argon Gas Stirred Ladle”, *ISIJ Int*., vol. 48, pp. 1704-1711, Sep. 2008.
45. U. Singh, R. Anapagaddi, S. Managal, K. A. Padmanabhan and A. K. Singh, “Multiphase Modeling of Bottom-Stirred Ladle for Prediction of Slag-Steel Interface and Estimation of Desulfurization Behaviour”, *Metall. Mater. Trans. B*, vol. 47, pp. 1804-1816, June. 2016.

46. H. Gonzalez, J. A. Ramos-Baderas, E. Torres-Alonso, G. Solorio-Diaz, C. A. Hernandez-Bocanegra, “Multiphase Modeling of Fluid Dynamic in Ladle Steel Operations Under Non-isothermal conditions”, *J. Iron Steel Res. Int*., vol. 24, pp. 888-900, Sep. 2017.
47. S. W. P. Cloete, J. J. Eksteen and S. M. Bradshaw, “A Mathematical Modelling Study of Fluid Flow and Mixing in Full-Scale Gas-Stirred Ladles”, *Prog. Comput. Fluid Dyn*., vol. 9, pp. 345-356, April. 2009.
48. S. W. P. Cloete, J. J. Eksteen and S. M. Bradshaw, “A Numerical Modelling Investigation into Design Variables Influencing Mixing Efficiency in Full Scale Gas Stirred Ladles”, *Miner. Eng*., vol. 46-47, pp. 16-24, May. 2013.
49. Q. Cao and L. Nastac, “Mathematical Investigation of Fluid Flow, Mass Transfer, and Slag-steel Interfacial Behaviour in Gas-stirred Ladles”, *Metall. Mater. Trans. B*, vol. 49, pp. 1388-1404, June. 2018.
50. Q. Cao and L. Nastac, “Numerical Modelling of the Transport and Removal of Inclusions in an Industrial Gas-stirred Ladle”, *Ironmaking & Steelmaking*, vol. 45, pp. 984-991, Jan. 2018.
51. T. Palovaara, V.-V. Visuri and T. Fabritius, ”Physical modelling of gas injection in a ladle”, *Proceedings of the 7th International Congress on Science and Technology of Steelmaking*, Associazione Italiana di Metallurgia, Venice, Italy, 2018.
52. K. Michalek, K. Gryc and J. Moravka, “Physical Modelling of Bath Homogenization in Argon Stirred Ladle”, *Metalurgija*, vol. 48, pp. 215-218, Oct. 2009.
53. S. Joo and R. I. L. Guthrie, “Modeling Flows and Mixing in Steelmaking Ladles Designed for Single-and Dual-plug Bubbling Operations”, *Metall. Mater. Trans. B*, vol. 23, pp. 765-778, March.1992.
54. M. S. C. Terrazas and A. Conejo, “Effect of Nozzle Diameter on Mixing Time during Bottom-Gas Injection in Metallurgical Ladles”, *Metall. Mater. Trans. B*, vol. 46, pp. 711-718, April. 2015.
55. A. N. Conejo, S. Kitamura, N. Maruoka and S.-J Kim, “Effects of Top Layer, Nozzle Arrangement, and gas Flow Rate on Mixing Time in Agitated Ladles by Bottom Gas Injection”, *Metall. Mater. Trans. B*, vol. 44, pp. 914-923. Aug. 2013.
56. S.-M. Pan, J.-D. Chaing and W.-S.Hwang, “Effects of Gas Injection Condition on Mixing Efficiency in the Ladle Refining Process”, *JMEPEG*, vol. 6, pp. 113-117. Feb. 1997.
57. J. Aoki, B. G. Thomas, J. Peter and K. D. Peaslee, “Experimental and Theoretical of Mixing in a Bottom Gas-Stirred Ladle”, *AISTech Proceedings*, Nashville, United States of America, September 15-17, 2004, pp. 1045-1056.
58. Q. Cao Q and L. Nastac, “Mathematical Modeling of the Multiphase Flow and Mixing Phenomena in a Gas-Stirred Ladle: The Effect of Bubble Expansion”, *JOM*, vol. 70, pp. 2071-2081, June. 2018.
59. W. Lou W and M. Zhu, “Numerical Simulations of Inclusion Behaviour and Mixing Phenomena in Gas-stirred Ladles with Different Arrangement of Tuyeres”, *ISIJ Int*., vol. 54, pp. 9-18, Aug. 2014.

60. D.-Q. Geng, H. Lei and Ji.-C. He, “Optimization of Mixing Time in a Ladle with Dual Plugs”, *Int. J. Min. Met. Mater*., vol. 17, pp. 709-714, Feb. 2010.
61. M. A. Ramirez-Argaez, “Numerical Simulation of Fluid Flow and Mixing in Gas-Stirred Ladles”, *Mater. Manuf. Process*., vol. 23, pp. 59-68, Dec. 2007.
62. T. Haiyan, G. Xiaochen, W. Guanghui and W. Yong , “Effect of Gas Blown Modes on Mixing Phenomena in a Bottom Stirring Ladle with Dual Plugs”, *ISIJ Int*., vol. 56, pp. 2160-2170, Oct. 2016.
63. M.-Y. Zhu, T. Inomoto, I. Sawada and T. Hsiao, “Fluid Flow and Mixing Phenomena in a Ladle Stirred by Argon through Multi-Tuyere”, *ISIJ Int*., vol. 35, pp. 472-479, Jan.1995.
64. H. Noureddini, B. C. Teoh and L. D. Clements, “Densities of Vegetable Oils and Fatty Acids”, *JAOCS*, vol. 69, pp. 1184-1188, Dec. 1992.
65. H. Noureddini, B. C. Teoh and L. D. Clements, “Viscosities of Vegetable Oils and Fatty Acids”, *JAOCS*, vol. 69, pp. 1189-1191, Dec. 1992.
66. N. Alia, M. Pylvänäinen, V.-V. Visuri, V. John and S. Ollila, “Vibrations of a laboratory-scale gas-stirred ladle with two eccentric nozzles and multiple sensors”, *J. Iron Steel Res. Int*., DOI: https://doi.org/10.1007/s42243-019-00241-x, 2019.
67. J. J. Valencia and P.N. Quested, “ASM Handbook”, vol. 15, pp. 468-481, Dec. 2013.
68. ANSYS Fluent Theory Guide, Release 17.1, Sep. 2006.
69. B.E. Launder and D. B. Spalding, “The Numerical Computation of Turbulent Flows”, *Comput. Meth. Appl. Mech*., vol. 3, pp. 269-281, Oct. 1974.
70. FactSage 7.2. GTT Gesellschaft für Technische Thermochemie und -physik mbH.
71. B. J. Keene, K. C. Mills, “Densities of molten slags”, In: Verein Deutscher Eisenhüttenleute: *Slag Atlas 2nd Edition*, Verlag Stahleisen GmbH, Düsseldorf, Germany, pp. 313-348. 1995.
72. J. W. Han, S. H. Heo, D. H. Kam, B. D. You, J. J. Pak and H.S. Song, “Transient Fluid Flow Phenomena in a Gas Stirred Liquid Bath with Top Layer Approach by Numerical Simulation and Water Model Experiments”, *ISIJ Int*., vol. 41, pp. 1165-1172, June. 2001.

Original publications

I Ramasetti, E.K., Visuri, V.-V., Sulasalmi, P., Kärnä, A., & Fabritius, T. (2017). Numerical study of multiphase flows in a ladle for different closure models. *Proceedings of the 11th Pacific Symposium on Flow Visualization and Image Processing, Kumamoto University, Kumamoto, Japan.*

II Ramasetti, E.K., Visuri, V.-V., Sulasalmi, P., & Fabritius, T. (2018). A CFD and experimental investigation of slag eye in gas stirred ladle. *Journal of Fluid Flow, Heat and Mass Transfer, 5*, 78-86.

III Ramasetti, E.K., Visuri, V.-V., Sulasalmi, P., Mattila, R., & Fabritius, T. (2019). Modeling of the effect of the gas flow rate on the fluid flow and open-eye formation in a water model of a steelmaking ladle. *Steel Research International, 90*(2), 1-15.

IV Ramasetti, E.K., Visuri, V.-V., Sulasalmi, P., Gupta, A.K., Palovaara, T., & Fabritius, T. (2019). Physical and CFD modelling of the effect of top layer properties on the formation of open-eye in gas-stirred ladles with single and dual-plugs. *Steel Research International, 1900088,* 1-13.

V Ramasetti, E.K., Visuri, V.-V., Sulasalmi, P., Savolainen, J., Li, M., Shao, L., & Fabritius, T. (2019). Numerical modelling of the influence of argon flow rate and slag layer height on open-eye formation in a 150-ton steelmaking ladle. *Metals, 9(10),* 1048.

VI Ramasetti, E.K., Visuri, V.-V., Sulasalmi, P., Fabritius, T., Saatio, T., Li, M., & Shao, L., (2019). Numerical modeling of open-eye formation and mixing time in argon stirred industrial ladle. *Metals, 9(8),* 829.

Original publications are not included in the electronic version of the dissertation.

695. Järvenpää, Antti (2019) Microstructures, mechanical stability and strength of low-temperature reversion-treated AISI 301LN stainless steel under monotonic and dynamic loading

696. Klakegg, Simon (2019) Enabling awareness in nursing homes with mobile health technologies

697. Goldmann Valdés, Werner Marcelo (2019) Valorization of pine kraft lignin by fractionation and partial depolymerization

698. Mekonnen, Tenager (2019) Efficient resource management in Multimedia Internet of Things

699. Liu, Xin (2019) Human motion detection and gesture recognition using computer vision methods

700. Varghese, Jobin (2019) MoO_3, PZ29 and TiO_2 based ultra-low fabrication temperature glass-ceramics for future microelectronic devices

701. Koivupalo, Maarit (2019) Health and safety management in a global steel company and in shared workplaces : case description and development needs

702. Ojala, Jonna (2019) Functionalized cellulose nanoparticles in the stabilization of oil-in-water emulsions : bio-based approach to chemical oil spill response

703. Vu, Kien (2019) Integrated access-backhaul for 5G wireless networks

704. Miettinen, Jyrki & Visuri, Ville-Valtteri & Fabritius, Timo (2019) Thermodynamic description of the Fe–Al–Mn–Si–C system for modelling solidification of steels

705. Karvinen, Tuulikki (2019) Ultra high consistency forming

706. Nguyen, Kien-Giang (2019) Energy-efficient transmission strategies for multiantenna systems

707. Visuri, Aku (2019) Wear-IT : implications of mobile & wearable technologies to human attention and interruptibility

708. Shahabuddin, Shahriar (2019) MIMO detection and precoding architectures

709. Lappi, Teemu (2019) Digitalizing Finland : governance of government ICT projects

710. Pitkänen, Olli (2019) On-device synthesis of customized carbon nanotube structures

711. Vielma, Tuomas (2019) Thermodynamic properties of concentrated zinc bearing solutions

Book orders:
Granum: Virtual book store
http://granum.uta.fi/granum/

UNIVERSITY OF OULU P.O. Box 8000 FI-90014 UNIVERSITY OF OULU FINLAND

ACTA UNIVERSITATIS OULUENSIS

UNIVERSITY of OULU
OULUN YLIOPISTO

ISBN 978-952-62-2355-1 (Paperback)
ISBN 978-952-62-2356-8 (PDF)
ISSN 0355-3213 (Print)
ISSN 1796-2226 (Online)